Nuclear structure of ^{229}Th from γ-ray spectroscopy study of ^{233}U α-particle decay

V. Barci,* G. Ardisson, G. Barci-Funel, B. Weiss, and O. El Samad
Laboratoire de Radiochimie et Radioécologie, Université de Nice, F06108 Nice Cédex 2, France

R. K. Sheline
Departments of Chemistry and Physics, Florida State University, Tallahassee, Florida 32306, USA
(Received 13 February 2003; published 30 September 2003)

The level structure of ^{229}Th, produced by α-particle decay of ^{233}U, was studied with γ-ray spectroscopy measurements. The sources were continuously separated from daughters with ion-exchange chromatographic methods. Singles and coincidence measurements were performed with high-purity germanium detectors. Energies and intensities of about 220 γ rays were accurately determined. About 70 transitions were reported for the first time, especially in the 300–700 keV energy range. A ^{229}Th level scheme was proposed, accounting for 220 transitions among 47 excited states. Alpha-particle feeding intensities and hindrance factors were deduced and compared to direct α-particle measurements; the agreement was found to be relatively good. The level structure was interpreted in the framework of rotational and/or reflection asymmetric models. The agreement with experimental data was shown to be satisfactory.

DOI: 10.1103/PhysRevC.68.034329 PACS number(s): 21.10.−k, 21.60.Ev, 23.60.+e

I. INTRODUCTION

The ^{229}Th nucleus is interesting for several reasons. First, the ground state (g.s.) and the first excited state are known to be almost degenerate: an excitation energy as low as 3.5 $\pm$1.0 eV was inferred by Reich and Helmer [1,2] from a careful investigation of energy differences between low energy levels connected by crossover transitions. This extremely low excitation energy has given rise to speculation about the possibility that external chemical and physical effects, such as molecular bonds and electronic configurations, might modify the nuclear properties, such as half-life and α-particle decay rate. Optical excitations of the isomer should also be possible, namely, by laser driven excitation [3]. No clear evidence of such events has been given so far [4]. For a recent review see Tkalya *et al.* [5] and references therein. A complete spectroscopy study of the low energy structure, accounting for all the transitions, has still not been accomplished and is attempted in this work.

Next, the nucleus ^{229}Th lies in the mass region where transitions from spherical to deformed shapes occur and asymmetric shapes are expected from theoretical studies. The existence of stable reflection asymmetric shapes in atomic nuclei was suggested in the 1980s, using energy calculations versus octupole deformation [6]. Afterwards many theoretical approaches were carried out for odd A nuclei in the mass range $\sim$219–229. Some models considered either adiabatic strong coupling of single particle orbitals to a deformed asymmetric core in a folded Yukawa potential [6,7]; others considered nonadiabatic coupling in deformed Woods-Saxon [8], or Nilsson potentials [9]. Dynamic octupole deformations involving a symmetric core coupled to asymmetric/anharmonic phonons [10] were also considered. The deformation parameters were assumed fixed for the whole nucleus [8] or the parameter set was minimized for each configuration [11]. Davydov-Chaban model calculations [12] were also carried out. For other theoretical discussions on the subject see also Refs. [13–16].

The parent ^{233}U ($T_{1/2}=1.592\times10^5$ yr) can be produced by successive β^- decays following thermal neutron capture in thorium, according to the reactions

$$^{232}\mathrm{Th}(n,\gamma)^{233}\mathrm{Th}\xrightarrow{\beta^-}{}^{233}\mathrm{Pa}\xrightarrow{\beta^-}{}^{233}\mathrm{U}.$$

The most complete works on γ-ray spectroscopy following ^{233}U α decay were performed by Kroger and Reich [17] and Canty *et al.* [18], with enriched and purified sources, and singles and coincidence measurements.

Energy and intensities of α particles were measured by Ahmad [19] and Glover [20] (see also the IAEA compilation of Ref. [21]). The agreement with the data deduced from γ ray and population intensity balances was poor. A possible explanation may be the existence of close unresolved doublets and multiplets. A careful analysis is carried out in this work.

Internal-conversion electron measurements are scanty [22], and probably affected by a systematic normalization factor, as pointed out by Kroger and Reich [17] (Sec. III B 1) and deduced from comparison with theoretical calculations [23].

The results and the references up to 1990 were gathered in the Nuclear Data Sheets compilation by Akovali [24].

The present work belongs to a series of papers following a research program developed at our laboratory on the level structures of the members of the $(4n+1)$ radioactive chain: ^{249}Cf [25,26], ^{241}Am [27], ^{233}Pa [28], ^{229}Th [29,30], ^{225}Ac [31], ^{221}Fr [32], ^{213}Bi, and ^{209}Tl [33]. Our research was partially motivated by the need for a better knowledge of the complex full spectrum of the chain in secular equilibrium with the anthropogenic nuclide ^{237}Np with the longest half-life ($T_{1/2}=2.14\times10^6$ yr). This isotope is the most critical product in nuclear waste from fission power plants and should be better known for future waste product treatment.

We present in Sec. II a review of our experimental methods, in Sec. III the γ-ray transition results and a revised level

*Electronic address: barci@unice.fr

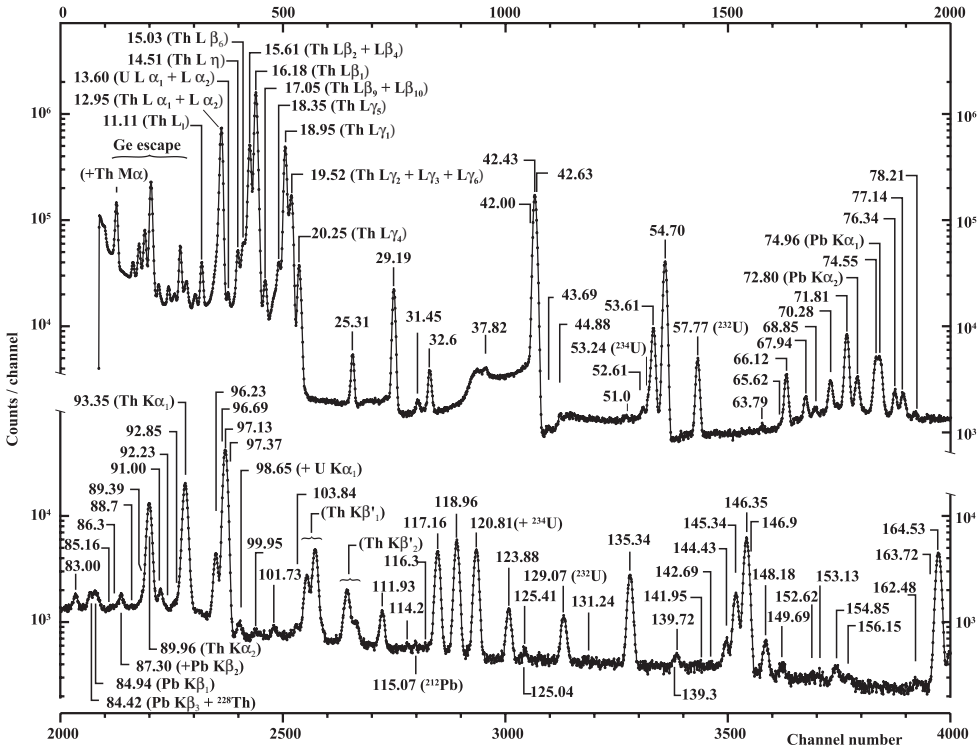

FIG. 1. A 68-h measurement of the ^{233}U source with the LEPS planar detector, 7 cm from source, 0.042 keV/ch. Background lines are marked by their corresponding emitting nuclide.

scheme of ^{229}Th, and in Sec. IV a discussion in the framework of the rotational model and a comparison with the predictions of some asymmetric models.

II. EXPERIMENTAL METHODS

A. Preparation of the ^{233}U source

The sources were obtained from two samples: a 10-mg sample from CEA (Centre d'Études Atomiques, Saclay), used for singles measurements, and a 100-mg sample from IPN (Institut de Physique Nucléaire, Orsay), 20-yr old, $>99.9\%$ isotopic purity according to the provider, used primarily for coincidence measurements. The ^{233}U samples were produced by neutron capture reaction on ^{232}Th in neutron reactor facilities. Nevertheless contaminating uranium isotopes (see Sec. III A 2), such as ^{232}U ($T_{1/2}=68.9$ yr) and ^{234}U ($T_{1/2}=2.455\times10^5$ yr), were present, and in spite of fast separation methods some of the daughters were also visible. These other U isotopes may have been produced by neutron reactions on ^{233}U in the reactor facility.

The samples were dissolved in 10 M HCl loaded into a Dowex® 1-X8 anionic column. Uranium isotopes, as UO_2^{2+}, were fixed as chlorocomplexes, while thorium and daughters were eluted. The column was washed with three column volumes of 10 M HCl. The eluate was evaporated to dryness. The measurements were started immediately afterwards, to minimize the daughters growing.

B. Detectors and measurements

Singles γ-ray measurements were performed with different detector and source assemblies.

(1) A planar low-energy photon spectrometer (LEPS) detector of 2 cm^3 active volume with an energy resolution, full width at half maximum (FWHM), of 190 eV at 6.4-keV (Fe K_α line), counting times of 68 h, was placed at 7-cm distance, with the 10-mg source (Fig. 1).

(2) A *p*-type coaxial high-purity germanium (HPGe) detector of 30% relative efficiencies and 1.9 keV energy resolution at 1.33 MeV (^{60}Co), with the 10-mg source, was used close to the detector, for 45-h counting time (Fig. 2).

(3) A second *p*-type coaxial HPGe detector of 40% efficiency and 1.9 keV energy resolution, 100 mg source, for 40 h, with two lead and one copper sheet each 1-mm thick as an absorber between the source and the detector, was used at 10 cm from the source.

(4) A more recent singles measurement was performed with a new coaxial HPGe *p*-type detector, 30% efficiency, 1.83-keV resolution, with the 10-mg source sample on top of the detector, for 160 h.

All counting sessions were performed with detectors shielded by a lead wall 5–10 cm thick. The combined results from different detector and source assemblies allowed to identify and eliminate summing effects.

Standard preamplifier-amplifier chains coupled to 8-K channel analyzers (EG&G Ortec) were used. The spectrometers were calibrated in energy and efficiency using standard sources: ^{241}Am, ^{152}Eu, ^{137}Cs, ^{133}Ba, ^{60}Co, and ^{57}Co. The reference values were taken from Ref. [34]. Internal calibrations were also performed using the accurate energy values measured by Helmer and Reich [2] for the strongest γ transitions in ^{229}Th level scheme.

Coincidence γ-ray measurements were performed with four HPGe detectors, three coaxial and one planar, placed at 90° to each other around the source, at about 15 cm. Typical resolutions were 1.8 keV (at 1.33 MeV ^{60}Co γ ray) for the coaxial detectors and 500 eV (at 122 keV ^{57}Co γ ray) for the

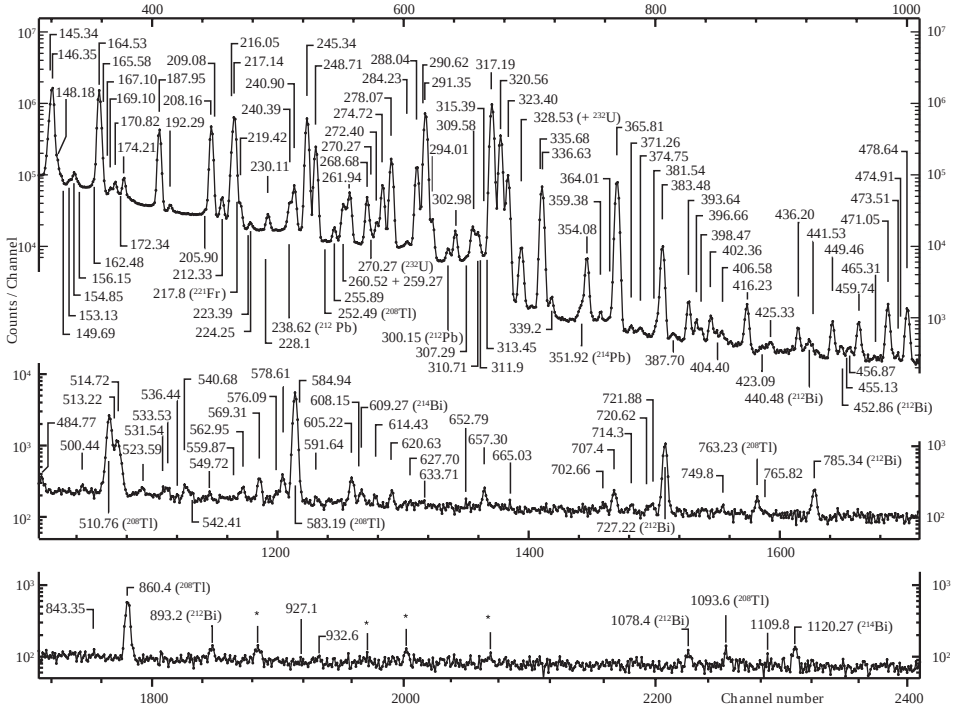

FIG. 2. Measurement of the pure ^{233}U 10-mg source, 45-h counting time, close to the 30% HPGe detector, 0.56 keV/ch. Background lines are marked by their corresponding emitting nuclide. Asterisks mark natural background lines.

planar detector; efficiencies were 17% for coaxial and 2% for planar detectors, respectively. Coincidence events with timing information were stored on tape and sorted afterwards. A total of 12.6×10^6 events were collected. Biparametric matrices within 150-ns time gate on prompt events were sorted for each pair of detectors. Some examples of coincidence spectra are shown in Fig. 3.

The analyses of γ-ray spectra were performed with the computer code GAMANAL [35]. Data processing was carried out with the utility and physics calculation codes of the program package provided by NNDC (National Nuclear Data Center, Brookhaven) [36]: HSICC, for theoretical internal-conversion electron coefficients from Hager and Seltzer's tables [23]; GTOL, for least squares fit of γ-ray energies and

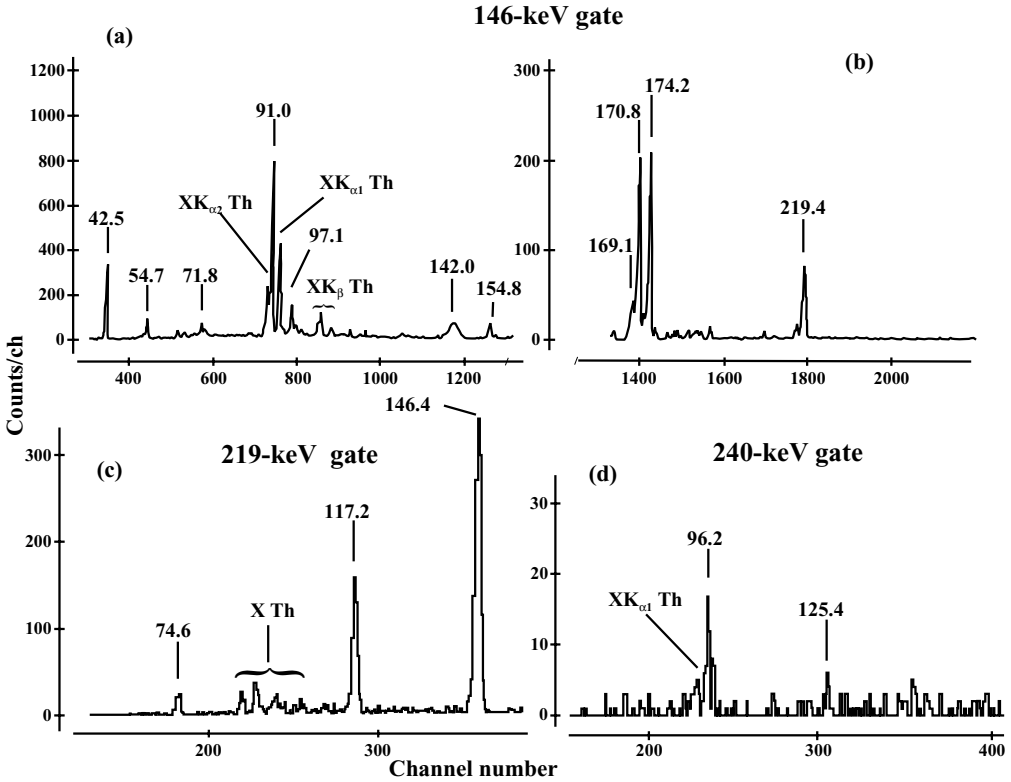

FIG. 3. Coincidence figures: (a,b) top, 146-keV gate; (c) bottom left, 219-keV gate, (d) bottom right, 240-keV gate. Gate widths are 2 keV, so multiple transitions were gated together, especially in the 146-keV gate.

intensities to level energies and intensity balances; ALPHAD, for Preston's [37] α-particle hindrance factor calculations, respectively.

III. RESULTS

A. Gamma-ray energies and intensities

1. Gamma-ray transitions

Energies and intensities of more than 200 γ-ray transitions were accurately measured. The intensities were normalized with respect to the 208.164-keV transition taken as 2.29 ± 0.03 per 10^5 decays as measured by Reich *et al.* [38]. The values are reported in Table I and compared to the adopted values of the compilation by Akovali [24] (mainly taken from Refs. [17,18,38]) and to those of Ref. [2]. The agreement between the different sets is generally good, apart from some weak transitions.

2. Contaminating γ rays

A careful analysis of the spectra was made to identify the γ lines coming from background, unseparated uranium isotopes, and daughter activities.

a. ^{234}U chain. The 53.236-keV line clearly corresponds to the 53.20-keV ^{234}U decay γ line [34]. This γ ray was misidentified with the 53.61-keV line from ^{233}U decay by Canty *et al.* [18]. The assignment to ^{234}U decay allows the subtraction of a weak contribution of the ^{234}U 120.90-keV line in the ^{233}U 120.8129-keV transition. Kroger and Reich [17] did not report the presence of ^{234}U in their source, but they did not separate the 53.20-keV line from the 53.61-keV line and their intensity of the 120.81-keV transition is much greater and disagrees with our value, so ^{234}U contamination was most likely present in their source.

Daughter activities were present as 185.96-keV (^{226}Ra); 295.12- and 351.92-keV (^{214}Pb); 609.27-, 1120.27-, 1237.5-, and 1765.42-keV (^{214}Bi) γ lines [34].

b. ^{232}U chain. The 57.770-keV line corresponds to the 57.78-keV ^{232}U decay γ line [34]. The associated 129.08-, 270.2-, and 327.9-keV lines are also observed at 129.070, 270.27, and 328.2 keV. The previously reported line at 129.4 keV by Kroger and Reich [17] and at 129.1 keV by Canty *et al.* [18] is mostly the ^{232}U line because the relative intensities of the other lines agree.

Daughter activities were identified at 84.416 keV (^{228}Th); 240.90 keV (^{224}Ra); 549.72 keV (^{220}Rn); 115.07, 238.619, and 300.148 keV (^{212}Pb); 288.037, 328.02, 452.86, 727.82, 785.34, 893.20 keV, and higher energy lines (^{212}Bi); 252.49, 272.25, 510.756, 583.190, and 763.226 keV (^{208}Tl).

The mass percent contaminations of ^{232}U and ^{234}U in the source could be estimated, respectively, as 7.7×10^{-8}% and 0.5%.

c. ^{233}U chain. Continuous separation and fresh preparation of the source have minimized the presence of the daughters: the main 193.52-keV ^{229}Th decay line (4.3% of the decay) [30] is at the detection limit, so we can assert that the 210.90-keV line belongs to the ^{233}U decay and is not the 210.89-keV ^{229}Th decay line (2.77%) [30] as assumed by Kroger and Reich [17]. Only the strongest transition of the chain: the ^{213}Bi line (26.1% of the decay [39]) can be clearly identified at 440.49 keV.

d. Natural background. In spite of the shielding used for every counting session, natural background (thorium, uranium, ^{40}K) was still present, especially at higher γ energies.

3. The 42-keV energy multiplet

The analysis of the 42-keV region of the γ-ray spectrum was carried out with particular care. It was undoubtfully known that at least two strong transitions: to the ground state and to the 29.19-keV energy level occurred in ^{229}Th. Helmer and Reich [2] showed that the 42-keV peak deviates from a pure one-Gaussian shape, which implies a weaker component on the high energy side. Our planar detector, with an experimental resolution of 0.34 keV in this range, allowed the separation of the two γ lines (Fig. 4).

The experimental separation was measured such as 0.1952 ± 0.0024 keV.

Some evidence occurs of a much weaker component in the low energy side, but this feature may be a deconvolution artifact. Coincidence measurements do not allow the separation of the multiplet, which is clearly correlated with most of the γ lines. The intensities of the different components were measured as 0.34, 72.0, and 13.2 per 10^5 decays of the parent. Our total intensity, 85.5 ± 3.6, agrees with the precise reference measurement of 86.2 ± 1.3 previously known [38].

A further component, corresponding to the transition between the 42.43-keV and 3.4-eV levels, may exist, but it cannot be separated by experimental methods. A possible deconvolution, on theoretical grounds, is discussed in Sec. IV A 4.

B. The ^{229}Th level scheme

1. Assignments: Energies and intensities

The ^{229}Th level scheme (Fig. 5) was built using the γ-ray data: the level energies were fitted to the energies of the transitions, mainly assigned according to coincidence relations. The γ gate at 42 keV was not retained at all in coincidence data: as previously discussed a strong multiplet matches almost every other γ ray. We confirmed most of the assignments of Kroger and Reich [17]; we also retained their assumption of the preferred feeding of the $3/2^+[631]$ band from negative parity states (see Sec. IV A 5), deduced from intensity considerations.

When the intensities were too weak and/or coincidences could not give the necessary information, energy differences were used to assign levels according to Ritz's principle.

Other measurements were taken into account to complete the level scheme.

(1) Internal-conversion electron (ce) measurements. As discussed in Ref. [17] the theoretical values [23] are roughly a factor of 2 larger than the experimental absolute values [22]; Reich and Helmer proposed a relative normalization on the L_{α_1} internal-conversion electron coefficient of the 97.13-keV *E2* transition, and assignments on K/L and L-subshell ratios, where available, to avoid normalization problems.

(2) Alpha-particle spectrum measurements [19–21,42].

TABLE I. Energies and intensities of γ transitions following the α-particle decay of ^{233}U. Uncertainties on the last digits of the value are given in parentheses.

This work		Previous work[a]		Placement[b]	Multipolarity[e]	Internal conversion
E_γ [c] (keV)	I_γ [d]	E_γ (keV)	I_γ [d]	$E_i - E_f$ (keV)		α[f]
(0.0034)	>2100[g]			0.0034–0	[$M1$]	
(13.244)	2.4[h] (7)			42.434–29.190	[$M1$]	380
20.25				(21–0)	[$E1$]	3.94
25.02 (5)	0.10 (4)			(237.355–212.305)	[$E1$]	4.66
25.311 (4)	2.11 (12)	25.3106[i] (8)	1.11 (17)	97.137–71.816	[$M1$]	227
	<0.004			173.469–148.154	[$M1$]	227
				(68-42.434)		
(27.119)	<0.002			173.469–146.350	[$E2$]	6240
(28.288)	0.036[h] (9)			125.425–97.137	[$M1$]	163
29.1867 (11)	7.8 (10)	29.1846[i] (30)	12.0 (3)	29.190–0.0034	$M1$ [+2%[h] $E2$]	235 (12)
(29.190)	2.7[h] (5)			29.190–0	[$M1$]	149
(29.382)	0.80[h] (14)			71.816–42.434	[$M1$]	149
31.449 (13)	0.24 (4)	31.52 (4)	0.25 (4)			
(32.453)	0.016[h] (3)			195.702–163.249	[$M1$]	109
32.57 (3)	0.018[j] (6)			288.472–255.917	[$M1$]	107
32.73 (5)	0.97 (12)	32.4 (2)	0.91 (14)	320.544–287.874	[$E1$]	2.33
36.516 (23)	0.14 (3)					
36.95 ((3)	0.12 (3)					
37.823 (16)	0.25 (4)	37.98 (12)	0.33 (5)	163.249–125.425	[$M1$]	69.0
42.005 (19)	0.34 (4)					
(42.431)	0.18[h] (5)			42.434–0.0034	[$E2$]	694
42.4344 (11)	72 (4)	42.4524[i] (7)	86.2 (13)	42.434–0	$M1$+16%[h] $E2$	1.4 (4)×10^2
42.6296 (21)	13.2 (7)			71.816–29.190	[$M1$+1.5%[h] $E2$]	58.0 (16)
43.69 (3)	0.042 (14)			255.917–212.305	[$M1$]	45.1
				(140–97.137)		
44.813 (21)	0.028[j,k] (9)			347.799–302.976	[$M1$]	41.8
(45.855)	0.0091[h] (16)			241.557–195.702	[$M1$]	39.1
51.0 (3)	0.03 (1)	50.5		287.874–237.355	[$M1$,$E2$]	1.6 (14)×10^2
52.607 (25)	0.10 (3)	52.62 (10)	0.23 (4)	217.156–164.530	[$M1$]	26.3
53.6104 (17)	3.47 (18)	53.6107[i] (11)	4.1 (5)	125.425–71.816	[$M1$+2%[h] $E2$]	28.3 (6)
54.7040 (11)	16.8 (8)	54.7038[i] (11)	18.2 (3)	97.137–42.434	$M1$+17%$E2$	55 (4)
				(75–21)		
63.79 (6)	0.029 (11)	63.88 (15)	0.03	237.355–173.469	[$M1$]	14.9
65.62 (5)	0.05 (1)			302.976–237.355	[$E1$]	0.364
				(140–75)		
66.116 (3)	1.02 (6)	66.1184[i] (6)	0.77 (12)	163.249–97.137	($M1$+24%[h] $E2$)	30 (9)
67.943 (7)	0.320 (23)	67.9460[i] (5)	0.29 (5)	97.137–29.190	[$E2$]	71.6
68.85 (6)	0.100 (23)	68.87 (5)	0.098 (18)	217.156–148.154	[$M1$]	11.9
70.281 (5)	0.58 (4)	70.2813[i] (13)	0.55 (8)	195.702–125.425	[$M1$+2.4%[h] $E2$]	12.4 (2)
71.8133 (16)	1.81[h,l] (14)	71.8159[i] (20)	2.4 (6)	71.816–0.0034	$E2$	54.9
	1.16[h,l] (12)			71.816–0	[$M1$+6%[h] $E2$]	13.1 (5)
	[l]			(374.789–302.976)		
(72.825)	<0.03[k]	72.88 (7)	0.54 (8)	237.355–164.530	[$E2$]	51.2
74.550 (6)	1.49 (8)	74.5390[i] (40)	1.50 (23)	146.350–71.816	[$E1$]	0.259
76.335 (10)	0.30[l] (3)	76.3507[i] (27)	0.36 (6)	148.154–71.816	[$E1$]	0.244
	<0.02[l,m]			173.469–97.137	[$E1$]	0.244
77.142 (8)	0.43[l] (4)	77.13 (4)	0.66 (10)	436.772–356.628	[$E1$]	0.237
	[l]			(272.5–195.702)	[$M1$+$E2$]	
78.21 (5)	0.044 (7)	78.15 (10)	0.055 (9)	241.557–163.249	[$M1$+24%[h] $E2$]	15.0 (15)
83.000 (13)	0.197 (22)	83.0128[i] (20)	0.16 (2)	125.425–42.434	[$M1$+28%[h] $E2$]	12.8 (14)
85.16 (5)	0.12 (4)	85.4224[i] (17)	0.17 (3)	320.544–235.34	[$E1$]	0.182
86.3 (3)	[l]	86.77 (15)	0.12 (3)	(235.34–148.1542)	[$M1$]	6.18
	0.038[h,l] (3)			327.8–241.557	[$M1$+16%[h] $E2$]	8.9 (5)

TABLE I. (*Continued.*)

This work		Previous work[a]		Placement[b]	Multipolarity[e]	Internal conversion
E_γ[c] (keV)	I_γ[d]	E_γ (keV)	I_γ[d]	$E_i - E_f$ (keV)		α[f]
	0.099[l] (23)			374.789–288.472	[$E2$]	23.0
87.30 (15)	0.088 (22)	87.27 (11)	0.17 (3)	212.304–125.425	[$E2$]	21.8
88.7 (2)	0.229 (23)	88.4746[i] (14)	0.40 (6)	235.34–146.350	[$M1$]	5.71
89.39 (7)	0.26 (3)			237.355–148.154	[$M1$]	5.58
90.999 (11)	0.31 (4)	91.03 (10)	0.30 (5)	237.355–146.350	[$M1$]	5.30
(91.433)	0.041[h] (7)			163.249–71.816	[$E2$]	17.5
92.23 (12)	0.033 (12)			347.799–255.916	[$M1$]	5.09
92.85 (3)	0.26 (3)			(187–97.137)		
96.232 (4)	1.70 (9)	96.244 (2)	1.27 (19)	125.425–29.190	[$E2$]	13.8
96.69 (7)	0.190 (25)					
97.1376 (11)	20.3 (10)	97.1344[i] (3)	20.3 (30)	97.137–0	$E2$	13.2
97.37 (4)	2.0 (6)			261.940–164.530	[$E1$]	0.129
(98.565)	0.097[h] (16)			195.702–97.137	[$M1+7\%$[h] $E2$]	4.74 (9)
99.95 (15)	0.019 (6)	100.03 (5)	0.050 (8)	317.176–217.156	[$E1$]	0.119
101.73 (3)	0.069 (15)	101.77 (7)	0.082 (13)	173.469–71.816	[$E1$]	0.114
103.84 (18)	0.063 (19)	103.6 (2)	0.092 (14)	320.544–217.156	[$E1$]	0.108
111.927 (7)	0.40 (3)	112.0 (1)	0.45 (5)	237.355–125.425	[$E1$]	0.383
114.2 (2)	0.183 (23)	114.4 (3)	0.23 (4)	287.874–173.469	[$M1$]	13.6
116.3 (2)	0.0047[l] (9)	116.41 (7)	0.19 (3)	241.557–125.425	[$E2$]	5.96
	0.121[l] (23)			436.772–320.544	[$E1$]	0.350
117.1575 (19)	2.87 (14)	117.1628[i] (9)	2.3 (4)	146.350–29.190	[$E1$]	0.344
118.9625 (17)	3.63 (18)	118.9721[i] (15)	4.06 (4)	148.154–29.190	($E1$)	0.331
120.8129 (19)	2.82 (15)	120.8194[i] (7)	3.32 (3)	163.249–42.434	$E2$	5.05
				(140–21)		
123.881 (5)	0.72 (5)	123.8860[i] (7)	0.59 (9)	195.702–71.816	[$E2$]	4.54
125.04 (23)	0.010 (3)			427.93–302.976	[$M1$]	10.4
125.41 (4)	0.051 (10)	125.41 (6)	0.060 (9)	125.425–0	[$E2$]	4.31
(129.514)	$\approx$0.06	129.25 (15)	0.064 (10)	(302.976–173.469)	[$E1$]	0.269
131.24 (10)	0.0174 (22)	131.1 (2)	0.030 (3)	173.469–42.434	[$E1$]	0.261
(132.1)	0.0035[h] (7)			327.8–195.702	[$E2$]	4.29
135.3394 (24)	1.97 (10)	135.3393[i] (5)	2.32 (2)	164.530–29.190	[$E1$]	0.242
139.3 (3)	[l]	138.5	0.014	374.789–235.34	[$E1$]	0.226
	0.0206[l] (23)			427.93–288.472	[$M1$]	7.68
139.720 (3)	0.090 (18)	139.7278[i] (45)	0.096 (15)	287.874–148.154	[$M1$]	7.61
141.95 (10)	0.0090 (15)	141.6		288.472–146.350	[$E1$]	0.216
142.69 (1)	0.034 (5)			359.628–217.156	[$E1$]	0.213
144.426 (14)	0.30 (3)	144.4 (2)	0.27 (4)	241.557–97.137	[$E2$]	2.39
145.342 (3)	1.73 (7)	145.337 (4)	1.5 (3)	217.156–71.816	[$E1$]	0.204
146.3462 (16)	6.5 (3)	146.3462[i] (6)	6.57 (6)	146.350–0.0034	($E1$)	0.201
146.9 (5)	0.116 (10)			(272.5–125.433)		
148.179 (10)	0.397 (20)	148.156 (8)	0.33 (5)	148.154–0	[$E1$]	0.195
149.691 (24)	0.095 (6)					
152.62 (10)	0.011 (3)	152.6		317.176–164.530	[$E1$]	0.182
153.13 (5)	0.037[l] (3)	153.1 (2)	0.050 (8)	195.702–42.434	[$E2$]	1.88
	[l]			(365.814–212.304)		
	[l]			(173.469–21)		
154.846 (22)	0.143 (8)	154.77 (12)	0.14 (2)	302.976–148.154	[$E1$]	0.176
156.15 (5)	0.036 (3)	156.14 (16)	0.053 (8)	320.544–164.530	[$E1$]	0.172
162.48 (3)	0.054[l] (5)	162.4 (2)	0.069 (11)	287.874–125.425	[$E1$]	0.157
	[l]			465.437–302.976		
163.72 (3)	0.117 (6)					
(164.5)	0.261[l] (5)			327.8–163.249	[$E2$]	1.41
164.534 (16)	6.0[l] (3)	164.5240[i] (5)	6.23 (5)	164.530–0.0034	($E1$)	0.152
165.581 (19)	0.407 (23)	165.7 (1)	0.35 (6)	237.355–71.816	[$E1$]	0.150

TABLE I. (*Continued.*)

This work		Previous work[a]		Placement[b]	Multipolarity[e]	Internal conversion
E_γ[c] (keV)	I_γ[d]	E_γ (keV)	I_γ[d]	$E_i - E_f$ (keV)		α[f]
167.10 (7)	0.0165 (14)			526.70–359.628	[$M1$]	4.58
169.10 (9)	0.041 (6)	169.002[i] (5)	0.062 (10)	317.176–148.154	[$E1$]	0.142
170.82 (3)	0.100 (6)	170.8091[i] (24)	0.13 (2)	317.176–146.350	[$E1$]	0.139
172.34 (10)	0.0228 (22)	172.36 (12)	0.032 (6)	320.544–148.154	[$E1$]	0.136
174.209 (18)	0.170 (9)	174.1919[i] (20)	0.21 (4)	320.544–146.350	[$E1$]	0.132
176.12 (5)	0.016 (5)	176.13 (7)	0.038 (6)			
177.94 (16)	0.0066[l] (13)	177.81 (6)	0.018 (3)	302.976–125.425	[$M1$]	3.83
	[l]			656.92–478.65		
184.1 (3)	0.022 (5)	184.3 (2)	0.023 (4)	425.891–241.557	[$E2$]	0.92
185.83 (11)	0.0078 (21)	185.81 (2)	0.037 (6)	(359.628–173.469)	[$E1$]	0.113
187.12 (3)	0.032 (4)					
187.953 (16)	1.87 (9)	187.9669[i] (3)	1.9 (3)	217.156–29.190	[$E1$]	0.110
188.65 (6)	0.025 (4)			425.891–237.355	[$E1$]	0.109
192.29 (6)	0.036 (4)	192.13 (4)	0.037 (6)	365.814–173.469	[$E1$]	0.105
198.60 (1)	0.0038 (13)					
205.90 (15)	0.0228 (24)	206.00 (12)	0.060 (9)	302.976–97.137	[$M1$]	2.54
				(526.70–320.544)		
207.25 (9)	0.032 (5)					
208.164 (16)	2.29 (11)	208.1795[i] (7)	2.29 (3)	237.355–29.190	[$E1$]	0.087
209.08 (8)	0.019 (3)			382.53–173.469		
210.90 (8)	0.0137 (24)			427.93–217.156	[$E1$]	0.085
212.332 (19)	0.130 (7)	212.34 (5)	0.126 (19)	212.304–0	[$M1$]	2.33
214.98 (11)	0.0058 (16)					
216.053 (17)	0.62 (3)	216.08 (10)	0.61 (9)	287.874–71.816	[$E1$]	0.0794
217.119 (16)	3.28 (16)	217.1519[i] (20)	3.2 (5)	217.156–0.0034	[$E1$]	0.0785
217.8 (2)	<0.003[k]	217.7	≈ 0.046	(365.814–148.154)	[$E1$]	0.0779
219.421 (18)	0.118 (6)	219.38 (5)	0.14 (3)	365.814–146.350	[$E1$]	0.0766
223.39 (6)	0.024 (3)	223.3 (2)	0.030 (4)	320.544–97.137	[$E2$]	0.452
224.39 (19)	0.0013 (4)	225.0 (3)	0.009 (2)	436.772–212.304	[$E1$]	0.0727
226.2 (2)	0.070 (23)	226.7 (3)	0.009 (2)	255.916–29.190	[$M1$]	1.96
230.11 (3)	0.071 (5)	230.11 (2)	0.062 (10)	425.891–195.702	[$M1+E2$]	1.1 (8)
230.97 (9)	0.0086 (22)					
237.51 (10)	0.0051 (17)					
240.388 (8)	0.413 (22)	240.3719[i] (17)	0.35 (6)	365.814–125.425	[$M1+E2$]	1.0 (7)
240.90 (4)	[k]			(382.53–140)		
244.50 (6)	0.038 (5)					
245.337 (16)	3.57 (18)	245.3498[i] (11)	3.62 (3)	317.176–71.816	($M1+E2$)	0.9 (7)
248.710 (16)	1.40[l] (7)	248.7242[i] (10)	1.43 (21)	320.544–71.816	($M1+E2$)	0.9 (6)
	[l]			569.255–320.544		
255.89 (3)	0.0393 (25)	255.94 (4)	0.039 (6)	255.916–0	[$M1$]	1.39
259.268 (19)	0.155 (8)	259.33 (4)	0.16 (3)	288.472–29.190	[$M1$]	1.34
260.52 (3)	0.102 (6)	260.65 (22)	0.098 (15)	302.976–42.434	[$M1$]	1.32
261.944 (18)	0.278 (14)	261.958[i] (4)	0.28 (5)	261.940–0.0034	[$M1$]	1.30
268.680 (18)	0.246 (12)	268.6747[i] (21)	0.23 (4)	365.814–97.137	[$M1+E2$]	0.7 (5)
272.40 (9)	0.071 (4)	272.34 (5)	0.057 (9)	436.772–164.530	[$E2$]	0.233
273.74 (5)	0.0155 (17)			302.976–29.190	[$M1$]	1.15
274.717 (17)	0.420 (22)	274.7347[i] (13)	0.40 (6)	317.176–42.434	[$M1+E2$]	0.7 (5)
278.070 (20)	1.13 (6)	278.1080[i] (9)	1.08 (17)	320.544–42.434	($M1+E2$)	0.7 (5)
284.23 (8)	0.0089 (16)	284.25 (15)	0.010 (1)			
287.32 (14)	0.015 (7)					
288.037 (25)	0.91 (5)	288.0292[i] (9)	0.97 (15)	317.176–29.190	[$M1+E2$]	0.6 (4)
				(605.237–317.176)		
288.50 (3)	0.117 (14)			288.472–0.0034	[$M1$]	0.99
290.62 (3)	0.109 (7)					

TABLE I. (*Continued.*)

This work		Previous work[a]		Placement[b]	Multipolarity[e]	Internal conversion
E_γ[c] (keV)	I_γ[d]	E_γ (keV)	I_γ[d]	$E_i - E_f$ (keV)		α[f]
291.353 (16)	0.62[j,l] (25)	291.3561[i] (9)	5.37 (5)	526.70–235.34	[$E1$]	0.0400
	4.63[l] (25)			320.544–29.190	($M1+E2$)	0.6 (4)
291.93 (4)	0.102 (15)			465.437–173.469		
294.006 (24)	0.122 (7)	293.995[i] (9)	0.13 (2)	365.814–71.816	[$M1+E2$]	0.6 (4)
302.978 (19)	[l]	302.990[i] (4)	0.084 (10)	374.789–71.8158	[$M1$]	0.87
	0.078[l] (4)			302.976–0[n]	[$M1$]	0.87
307.29 (16)	0.0050 (14)			569.255–261.940		
309.58 (12)	0.083 (5)	309.5 (2)	0.066 (10)	526.70–217.156	[$E1$]	0.0350
310.71 (5)	0.038 (3)			382.53–71.816		
311.9 (3)	0.063 (4)	312.0 (5)	0.025 (10)	436.772–125.425	[$E1$]	0.0344
313.45 (18)	0.0056 (11)			569.255–255.916		
315.39 (13)	0.0100 (15)			478.65–163.249	[$M1$,$E2$]	0.5 (4)
316.30 (4)	0.094 (7)					
317.191 (16)	7.1[l] (4)	317.1689[i] (15)	7.76 (7)	317.176–0[n]	($M1+E2$)	0.5 (3)
	0.27[l] (11)			359.628–42.434	[$M1$]	0.765
320.560 (16)	2.78 (14)	320.5471[i] (13)	2.90 (3)	320.544–0[n]	($M1+E2$)	0.4 (3)
323.396 (16)	0.77 (4)	323.3806[i] (14)	0.77 (12)	365.814–42.434	[$M1+E2$]	0.4 (3)
328.53 (12)	0.080 (4)	328.758[i] (5)	0.060 (9)	425.891–97.137	[$M1+E2$]	0.4 (3)
335.68 (8)	0.0081 (19)					
336.631 (16)	0.58 (3)	336.6195[i] (16)	0.54 (8)	365.814–29.190	[$M1+E2$]	0.4 (3)
339.2 (6)	0.0025 (16)	338.9 (5)	0.007 (3)	436.772–97.137	[$E1$]	0.0286
354.082 (20)	0.060 (4)	354.03 (3)	0.053 (8)	425.891–71.816	[$M1+E2$]	0.34 (23)
359.38 (19)	0.0049 (15)			359.628–0[n]	[$M1$]	0.544
364.01 (12)	0.0064 (16)			(605.237–241.557)		
365.820 (16)	0.77 (4)	365.8206[i] (35)	0.75 (12)	365.814–0[n]	($M1+E2$)	0.31 (22)
371.26 (23)	0.0014 (7)			536.30–164.530	[$M1$]	0.498
374.7 (3)	0.0038 (20)			374.789–0[n]	[$M1$]	0.486
381.54 (15)	0.0039 (13)			478.65–97.137	[$M1$]	0.463
383.482 (21)	0.096 (5)	383.47 (8)	0.087 (13)	425.891–42.434	[$M1+E2$]	0.27 (19)
387.76 (12)	0.0012 (3)			513.401–125.425		
393.64 (5)	0.0130 (12)	393.70 (15)	0.007 (3)	465.437–71.816		
396.64 (13)	0.0044 (10)	396.7 (1)	0.008 (1)	425.891–29.190	[$E2$]	0.0775
402.36 (9)	0.0072 (14)	402.4 (2)	0.008 (3)	637.45–235.34		
404.33 (19)	0.0013 (4)			569.255–164.530		
406.58 (16)	0.0015 (4)	406.7 (3)	0.0050 (5)	478.65–71.816	[$M1$]	0.390
416.24 (3)	0.0120 (10)	416.4 (2)	0.009 (3)	513.401–97.137		
423.09 (14)	0.00052[l] (14)			465.437–42.434		
	[l]			569.255–146.350		
425.33 (12)	0.00080 (14)			637.45–212.304		
436.20 (12)	0.0035[l] (9)	436.6 (4)	0.0048 (7)	465.437–29.190		
	[l]			478.65–42.434		
441.53 (17)	0.00073 (22)			513.401–71.816		
449.46 (7)	0.0064 (8)	449.5 (2)	0.008 (3)	478.65–29.190	[$M1$]	0.297
455.13 (11)	0.00117 (21)			526.70–71.816	[$M1$]	0.288
456.87 (16)	0.00044 (21)			605.237–148.154		
459.74 (6)	0.0076 (11)	459.8 (2)	0.0080 (8)	585.09–125.425		
465.37 (12)	0.00047 (23)			465.437–0[n]		
471.05 (4)	0.0185 (18)	471.2 (2)	0.014 (2)	513.401–42.434		
473.51 (18)	0.0030 (15)					
474.41 (8)	0.00077 (11)			620.79–146.350		
478.64 (4)	0.0148 (12)	478.6 (2)	0.014 (2)	478.65–0[m]	[$M1$]	0.251
484.8 (3)	0.0023 (10)	484.1 (2)	0.004 (1)	526.70–42.434	[$M1$]	0.243
500.44 (23)	0.00070 (23)			665.02–164.530		
513.23 (13)	0.0165[l] (21)			513.401–0[n]		

TABLE I. (*Continued.*)

This work		Previous work[a]		Placement[b]	Multipolarity[e]	Internal conversion
E_γ[c] (keV)	I_γ[d]	E_γ (keV)	I_γ[d]	$E_i - E_f$ (keV)		α[f]
	[l]			585.09–71.816		
514.72 (13)	0.0112 (18)	514.0 (5)		749.91–235.34		
523.59 (24)	0.00094 (24)			620.79–97.137		
531.54 (8)	0.00070 (23)			656.92–125.425		
533.53 (5)	0.00117 (23)			605.237–271.816		
536.44 (12)	0.00047 (23)	537.5 (5)		536.30–0.0034	[$E1$]	0.0110
540.68 (13)	0.00164 (23)	540.3 (2)	0.0050 (5)	637.45–97.137		
542.41 (13)	0.00047 (23)	545.1 (3)	0.0023 (2)	585.09–42.434		
559.87 (18)	$\approx$0.00023			656.92–97.137		
562.95 (24)	0.0014 (7)	562.8 (5)		605.237–242.434		
569.31 (16)	0.0039 (15)	569.4 (2)	0.0036 (4)	569.255–0 [n]		
576.09 (20)	0.0009 (4)			605.237–229.190		
578.61 (17)	0.0034 (11)	578.5 (2)	0.0049 (5)	620.79–42.434		
584.94 (16)	[l]			656.92–71.816		
	$\approx$0.00023[l]			585.09–0 [n]		
591.6 (3)	0.00070 (23)			620.79–29.190		
605.22 (13)	0.0048 (9)			605.237–0 [n]		
608.15 (5)	0.00047 (23)			637.45–29.190		
614.60 (20)	0.00070 (23)			656.92–42.434		
620.63 (23)	0.0015 (6)	620.9 (2)	0.0022 (3)	620.79–0 [n]		
627.70 (8)	0.00047 (23)			656.92–29.190		
633.51 (12)	0.00069 (23)					
637.25 (10)	$\approx$0.00023			637.45–0 [n]		
652.79 (19)	$\approx$0.00023			749.91–97.137		
657.30 (17)	0.0040 (10)	657.0 (2)	0.0028 (3)	656.92–0 [n]		
665.03 (10)	$\approx$0.00023			665.02–0 [n]		
702.7 (3)	0.0011 (5)					
707.4 (3)	0.0020 (9)	707.5 (2)	0.0027 (3)	749.91–42.434		
714.3 (3)	0.00047 (23)					
720.62 (11)	0.00047 (23)			749.91–29.190		
721.88 (14)	0.0040 (11)					
749.8 (4)	0.00047 (23)			749.91–0 [n]		
765.82 (20)	0.00014 (7)					
843.35 (10)	0.00016 (5)					
927.1 (3)	0.0014 (7)					
932.6 (3)	0.0014 (7)					
1109.8 (5)	0.0008 (3)					

[a]Reference [24] unless otherwise stated.

[b]Unassigned transitions have blank placements; uncertain placements are in parentheses.

[c]Values in parentheses are transitions not observed, but required from coincidence relations, intensity balance or rotational model calculations.

[d]Relative intensity for 10^5 α-particle decays of the parent.

[e]Values in square brackets are from spin-parity values: they were not measured; values in parentheses are deduced from indirect or uncertain measurements.

[f]Theoretical internal-conversion electron coefficients from Ref. [23]. Uncertainties account for those of mixing ratios.

[g]Total intensity limit required from intensity balance. No conversion process is allowed because the energy is lower than the lowest available electron excitation energy.

[h]Calculated from strong coupling rotational model (see Sec. IV A 4).

[i]From Ref. [2].

[j]Calculated from intensity balance.

[k]Intensity components from room background, other uranium isotopes, and daughter radiation were subtracted.

[l]Multiply placed transition: intensity suitably divided or assigned, as discussed in the text.

[m]From general trend of transition intensity to levels of the same band.

[n]The final level is uncertain: the g.s. is assumed, but may be the 3.4-eV level.

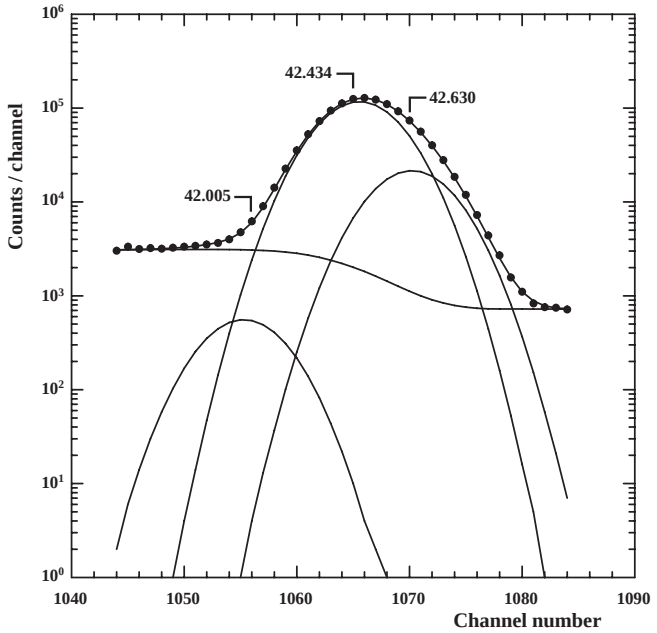

FIG. 4. Deconvolution of the 42-keV multiplet. Dots are experimental counts.

(3) (d,t) reaction [43].

(4) ^{229}Ac β^- decay and ^{229}Pa ϵ decay [44,45] (as reported by Akovali [46]).

New levels were retained only if at least three experimental relations to the level existed: transitions into and out of the level, or other measurements; with only two relations the level was considered uncertain.

When the transitions to the g.s. doublet could not be clearly separated and assigned only once, they were assigned only to the g.s.: the energy uncertainties were always greater than the energy separation of the doublet and do not invalidate the fitting procedure. We may point out that the general fit of all the γ lines to the whole level scheme is in very good agreement with the results of Helmer and Reich [2]: the energy of the first excited level obtained in the fit is 3.4 $\pm$1.8 eV.

Many transitions are multiply placed: in some cases they could be resolved using the complementary experimental data. If no assignment could be made, the intensity was arbitrarily assigned to the transition between the lowest excited states. Finally, the low energy multiplets were separated according to the theoretical discussion of Sec. IV A 4.

2. Spins and parities

The spins and parities of the levels were primarily deduced in a model-independent way, allowing only $E1$, $M1$, and $E2$ multipolarities for the observed γ-ray transitions, following the usual selection rules, and according to the measured internal-conversion electron coefficients [22] if available. $E1$ assignments for strong γ-ray transitions were based on the absence of the corresponding transitions in the electron spectra. For some of the low-intensity γ rays, we assumed the lowest multipolarity allowed by the level scheme. In no case were these multipolarities used to establish spins and parities of levels.

3. Alpha-particle feedings and hindrance factors (HF)

The α-particle transition intensities feeding the levels. were calculated from the total $\gamma+$ce intensity imbalances at each level (Table II).

The agreement of the γ-ray intensity balances with the α spectrum, primarily from Ref. [42], reported in the compilation of Akovali [24], and from other references therein, is reasonably good. The uncertainties for the γ-ray intensity balances mainly come from incomplete knowledge of transition multipolarities. Weak feedings undetected in experimental α-particle spectra are reported to some high energy excited levels. Hindrance factors for α-particle branches were calculated according to the spin-independent equations of Preston [37], from the used α-particle feedings.

4. New levels

We only discuss levels with new properties or major changes with respect to previous data [17,18] and as far as possible in a model-independent way. Since ^{229}Th is relatively well deformed (Sec. IV A 1) the rotational model is also helpful.

The 186.6-keV level proposed in Ref. [17] is not confirmed: the 236.3 γ ray from the 425.87-keV level is not observed.

The 235.5-keV level proposed by Canty *et al.* [18] is confirmed: the deexciting transitions are very weak, but three new transitions into the level could be assigned.

We propose a level at 272.5 keV, which might account for the 77.14- and 146.9-keV transitions. It may be the next level, $13/2^+$, of the $3/2^+[631]$ band (see also Sec. IV A 2).

The 327.8-keV level is proposed as the $15/2^+$ member of the g.s. band (see Sec. IV A 1).

The 340- and 466.9-keV levels proposed by Canty *et al.* [18] are not confirmed: none of the γ rays assigned by these authors was clearly observed.

The 347.80-, 374.79-, 427.93-keV levels were observed in α-particle decay. Two, five, and two transitions, respectively, can be assigned to these levels.

The 359.63-, 382.53-, and 536.30-keV levels may correspond to levels observed in the ^{230}Th(d,t) reaction (Ref. [47] cited in Nuclear Data Sheets [46]). Four, two, and two transitions, respectively, can be assigned to these three levels.

The 436.77- and 465.44-keV levels proposed by Kroger and Reich [17] and/or Canty *et al.* [18] are confirmed by assigning half-a-dozen transitions each.

New levels are proposed at 513.40, 585.09, 620.79, 637.45, 665.02, and 749.1 keV by assigning two or more transitions each.

The levels at 569.26 and 605.24 keV, observed in β^- decay of ^{229}Ac, were also observed in α decay.

IV. DISCUSSION AND COMPARISON WITH THEORY

A. Rotational symmetric models

1. The g.s. band

The levels of the $5/2^+[633]$ g.s. band up to $13/2^+$ were known from previous studies [17,18].

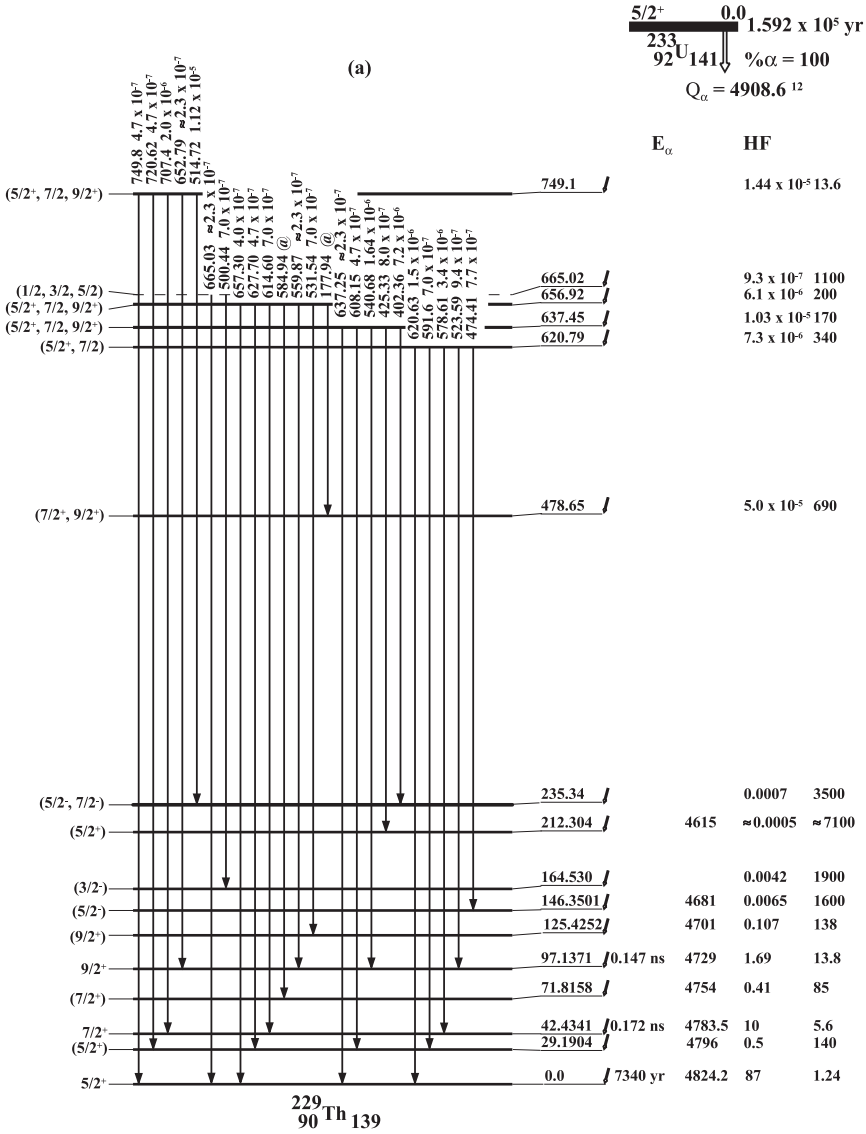

FIG. 5. The ^{229}Th level scheme. We report total intensities $I_{\gamma+ce}$ per 100 decays of the parent. Transition marked by an ampersand are multiply placed, with intensities suitably divided. Closed circles mark coincidence relations; dotted lines mark uncertain placements. Alpha-particle energies are experimental values from Refs. [19,20]. The decay Q value is from Ref. [40]. Half-lives are from Ref. [41].

It was proposed [24] that the 85.16-keV transition could be the $15/2^+ \rightarrow 13/2^+$ transition of the g.s. band. This assignment is almost certainly wrong: the $\Delta I=2$ intraband transition $15/2^+ \rightarrow 11/2^+$ should be stronger according to the rotational model (see Sec. IV A 4), but no evidence exists of a 163.5-keV crossover transition in the experimental spectrum. A better hypothesis is to identify the $15/2^+ \rightarrow 13/2^+$ transition with the 86.3-keV γ line, which would then be multiply placed. By combining the experimental value of the α-particle feeding of the 327.0-keV level with the ratio between $M1$ and $E2$ transition strengths, deduced from the rotational model, we calculated the intensities of the $\Delta I=1$ and $\Delta I=2$ transitions. The latter, 164.5 keV from energy level difference, may be hidden below the much stronger 164.534-keV γ line (intensities 0.261 versus 6.0 for a total experimental intensity of 6.3 ± 0.3 per 10^5 decays of the parent).

The band parameter, deduced from a least squares fit to the energies of the levels, is $A=6.06$ keV, with a one-parameter fit and a root-mean-square deviation (rms) of 0.34 keV.

From Table III the values of the intrinsic quadrupole moment and gyromagnetic ratio calculated from the experimental matrix elements and the rotational formula for the reduced transition probabilities [48] agree within the experimental uncertainties. Nevertheless, the data for the 42.434-keV transition are less reliable because the γ line is a multiplet (see Sec. IV A 4).

Weighted mean values $Q_{20}=7.1\pm0.3$ b and $|g_K-g_R|=0.176\pm0.021$ can be obtained. The model is consistent with the data and we are confident in applying the Alaga's rule. However, the measured spectroscopic quadrupole moment 4.3 ± 0.9 b, from hyperfine structure [49], or 3.1 b, from Coulomb excitation [50], does not agree very well with the value (2.5 b) calculated in the strong coupling limit. The experimental magnetic moment $[\mu=(+0.45\pm0.04)\mu_N]$ [49] was correctly reproduced ($\mu=0.4\mu_N$) in the framework of the strong coupling model, with matrix elements calculated with a Woods-Saxon potential for $\epsilon_2=0.19$ [51], but it may be a chance agreement: the calculated $g_K-g_R=-0.31$ strongly disagrees.

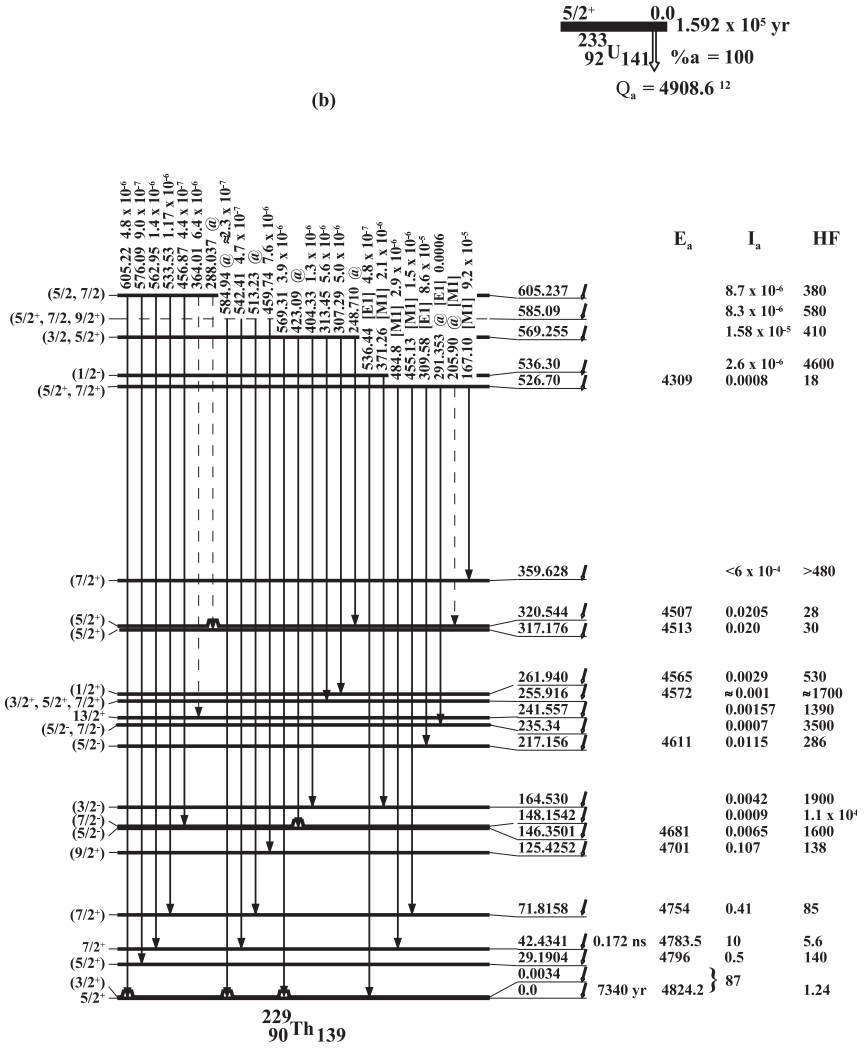

FIG. 5. (*Continued.*)

From the quadrupole moment we can calculate the effective quadrupole deformation $\overline{\epsilon_2}=0.169$, which agrees with the values for the neighboring even-even isotopes ^{228}Th (0.146) and ^{230}Th (0.182), deduced from the half-lives of the corresponding first excited 2^+ states [52,53]. This effective deformation corresponds to a deformation parameter [8] $\epsilon_2 \sim 0.16$.

We can also infer the value of the magnetic g factor from the relation

$$|\delta| = 9.33\times 10^{-4}\frac{E}{\sqrt{(I-1)(I+1)}}\left|\frac{Q_{20}}{g_K-g_R}\right| \qquad (1)$$

for the experimental mixing ratio, with the transition energy E in keV and Q_{20} in barn, of the intraband $I\rightarrow I-1$ transitions. From Table IV the value of Q_{20} and the weighted mean value of $|Q_{20}/(g_K-g_R)|=40.1\pm 2.4$ b we have $|g_K-g_R| = 0.177\pm 0.013$, in agreement with the value deduced from the measured reduced matrix elements.

2. The 3/2+[631] band

The $3/2^+[631]$ band was proposed and carefully discussed by Kroger and Reich [17].

The band parameters, deduced from a least squares fit to the level energies, are $A=6.05$ keV (one-parameter fit, rms $=1.26$ keV), or, better, $A=5.78$ keV, $A_3=0.15$ eV (two-parameter fit, rms$=0.49$ keV). From the values of the inertia parameter we can assume that the deformations of the $3/2^+[631]$ and g.s. bands are almost equal; the slightly lower value may indicate a low Coriolis interaction (Sec. IV A 3). The need for an alternating term points to the existence of signature-dependent effects.

We propose the identification of the $13/2^+$ member of the band with a 272.5-keV level, from the existence of two γ-ray lines of 77.14 and 146.9 keV, interpreted as the $\Delta I=1$ and $\Delta I=2$ intraband transitions. The excitation energy is in good agreement with the rotational formula. The former transition belongs to a doublet, the latter is strongly hidden by the close 146.34-keV transition.

In Table V we derived the mixing ratios by applying the Alaga's rule to transitions issuing from the same level. From

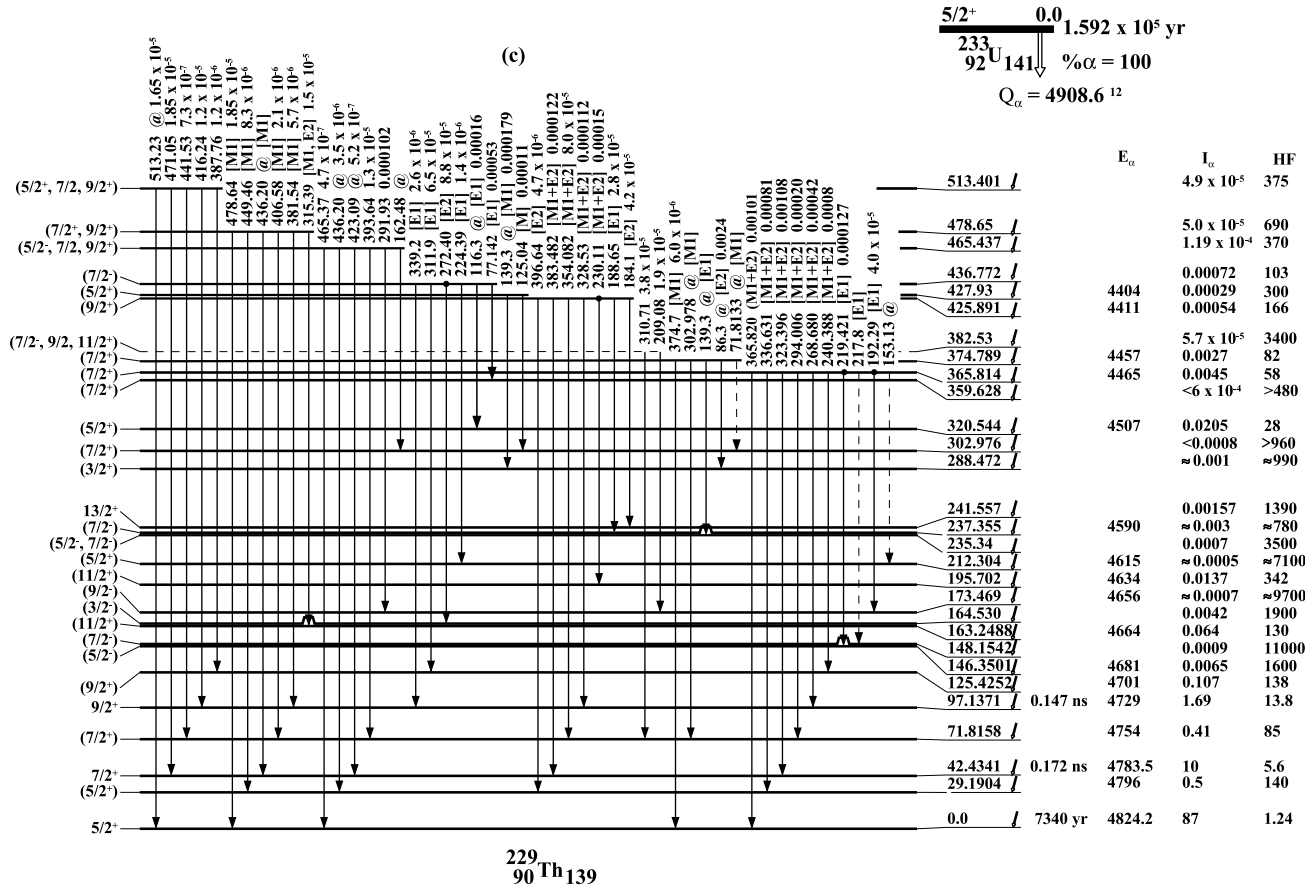

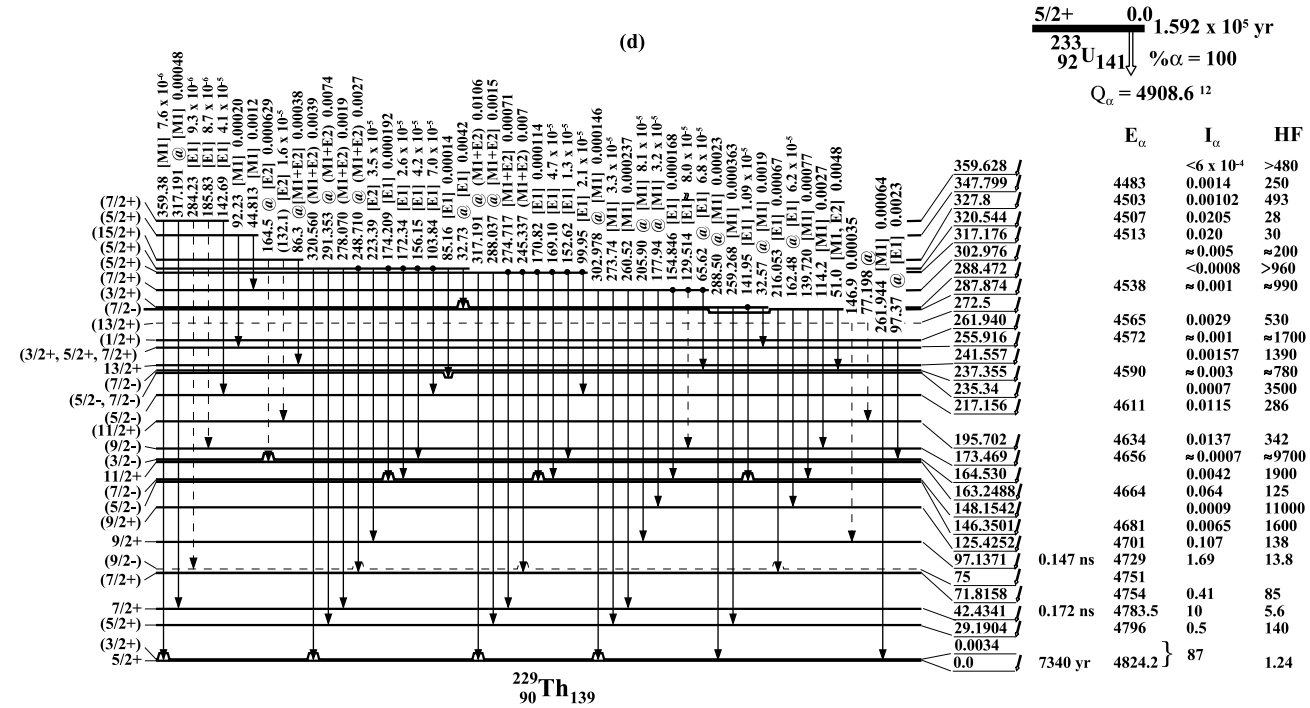

FIG. 5. (*Continued.*)

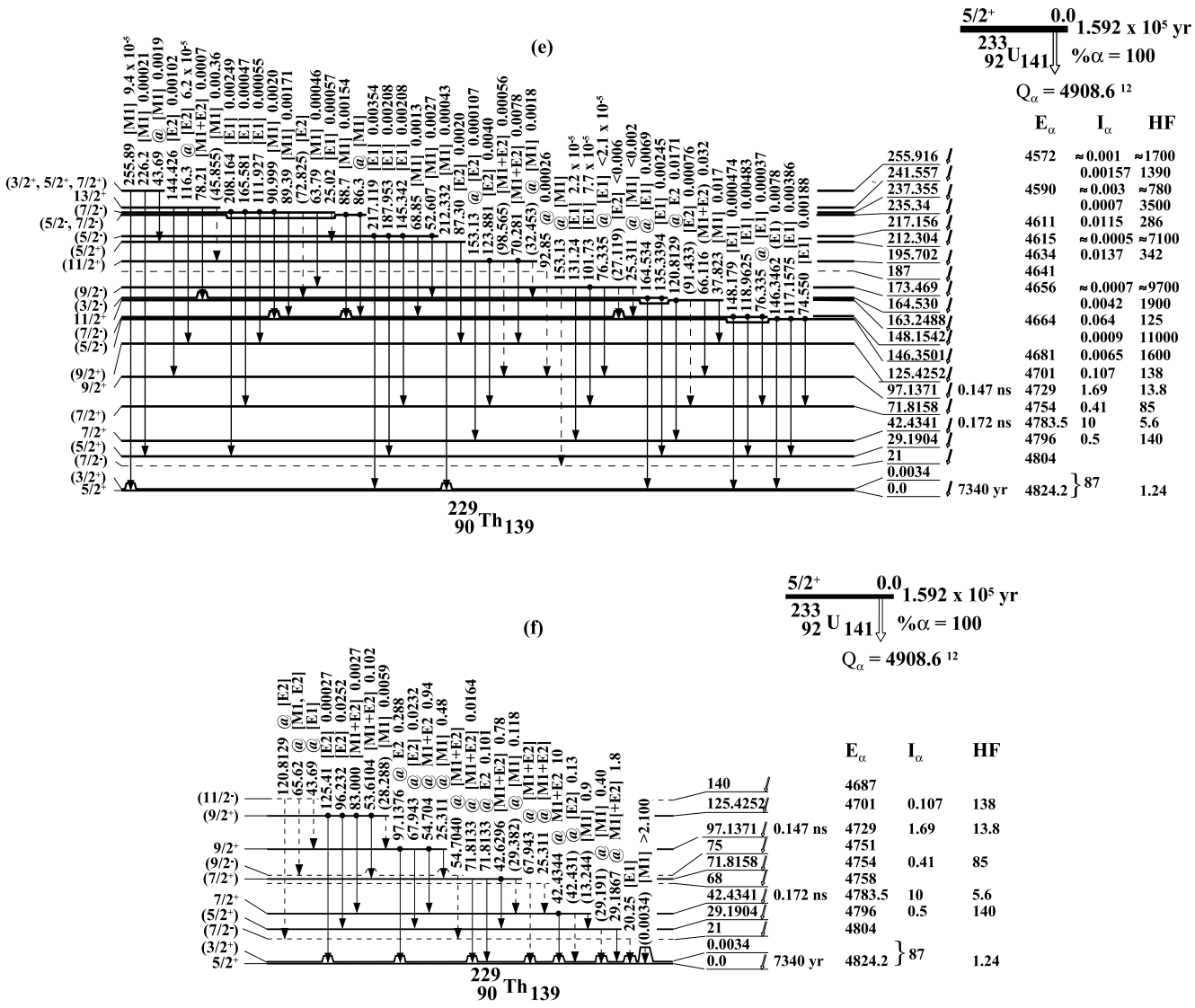

FIG. 5 (*Continued*).

Eq. (1), with the value of Q_{20} of the g.s. band and the weighted mean $|Q_{20}/(g_K-g_R)|=12.8\pm0.4$ b we have $|g_K-g_R|=0.56\pm0.03$ for the $3/2^+[631]$ band. This value is in good agreement with the calculated value $g_K-g_R=-0.61$ of Ref. [51].

3. Coriolis mixing

Several experimental features suggest that Coriolis mixing between the close $5/2^+[633]$ and $3/2^+[631]$ bands is low or negligible.

(1) The hindrance factor of the α transitions to levels of the $3/2^+[631]$ band is high: the intensity to the 5/2, 7/2, and 9/2 members of the $3/2^+[631]$ band should be strong even for moderate mixing, because the $5/2^+[633]$ band is the favored band.

(2) The energy difference between like spin levels is nearly constant: it would increase with spins if the bands were mixed.

(3) The calculation of the mixing for a two-band interaction gives unphysical results.

We estimated the mixing from the intensity ratio of the 97.14- and 67.94-keV $E2$ transitions from the $9/2^+$ member of the g.s. band. The former, intraband, is purely rotational; the latter, interband, contains an intrinsic, single-particle, term and a rotational term depending on Coriolis mixing. The intrinsic transition $5/2^+[633]\leftrightarrow3/2^+[631]$ violates $E2$ selection rules ($\Delta n_3=1,\Delta\Lambda=1,\Delta\Sigma=0$) for Nilsson asymptotic configurations, so the matrix element may be assumed negligible. With $A=6.06$ keV for the inertia parameter; $E_{K+1}-E_K\approx6$ keV for the intrinsic energy difference, and pairing factor $P_{K+1,K}=u_Ku_{K+1}+v_Kv_{K+1}\approx1$, where $u\approx v\approx2^{-1/2}$, because the two bands are very close to the Fermi level, we obtain $\langle5/2[633]|\hat{J}_+|3/2[631]\rangle f=0.069$, which is strongly reduced ($f=0.15$) relative to the theoretical value 0.46 [51]. This reduction is not uncommon in this region: in the near nucleus ^{233}U the reduction of the coupling strength between the two bands was found to be 0.21 [54].

With (d,t) particle reaction spectroscopy Burke *et al.* [43] have clearly established the existence of a $1/2^+[631]$ band with levels at 262 ($1/2^+$), 288 ($3/2^+$), and maybe 310

TABLE II. I_{total} imbalances compared with I_α's.

E_{level} (keV)	I^π	Feeding intensity (%)		Hindrance factor	
		This work	From α spectra[a]	This work	From α spectra[a]
0	$5/2^+$	87[b] (3)	84.4[b] (5)	1.24	1.3
0.0034 (18)	$(3/2^+)$				
21	$(7/2^-)$		0.051[c]		1530
29.1904 (18)	$(5/2^+)$	0.5 (4)	0.28	140	240
42.4341 (9)	$7/2^+$	10 (3)	13.2 (2)	5.6	4.2
68			0.016[c]		2320
71.8158 (14)	$(7/2^+)$	0.41 (7)	0.163	85	210
75	$(9/2^-)$		0.01[c]		3320
97.1371 (9)	$9/2^+$	1.69 (10)	1.61	13.8	14
125.4252 (20)	$(9/2^+)$	0.107 (8)	0.06	138	250
140	$(11/2^-)$		0.0028[c]		4170
146.3501 (21)	$(5/2^-)$	0.0065 (17)	0.01[d]	1600	1050
148.1542 (24)	$(7/2^-)$	0.009 (7)		11000	
163.2488 (18)	$11/2^+$	0.064 (10)	0.042[e]	125	190
164.530 (3)	$(3/2^-)$	0.0042 (12)		1900	
173.469 (5)	$(9/2^-)$	($\approx$0.0007[f])	$\approx$0.005	($\approx$9700)	$\approx$1350
187			0.003[c]		1800
195.702 (4)	$(11/2^+)$	0.0137 (8)	0.01	342	470
(202)			$\leqslant$0.004[c]		$\geqslant$1050
212.304 (17)	$(5/2^+)$	$\approx$0.0005	0.04	$\approx$7100	890
217.156 (4)	$(5/2^-)$	0.0115 (9)	0.006	286	550
235.34 (4)	$(5/2^-,7/2^-)$	0.0007(3)	0.007[g]	3500	355
237.355 (6)	$(7/2^-)$	$\approx$0.003		$\approx$780	
241.557 (14)	$13/2^+$	0.00157(18)		1390	
255.916 (19)	$(3/2^+,5/2^+,7/2^+)$	$\approx$0.001	0.0023	$\approx$1700	745
261.940 (17)	$(1/2^+)$	0.0029 (7)	0.0028	530	550
287.874 (4)	$(7/2^-)$	$\approx$0.005	0.004[h]	$\approx$200	250
288.472 (15)	$(3/2^+)$	$\approx$0.001		$\approx$990	
302.976 (10)	$(7/2^+)$	$<$0.0008		$>$960	
317.176 (9)	$(5/2^+)$	0.020 (4)	0.018	30	34
320.544 (8)	$(5/2^+)$	0.0205 (24)	0.012	28	47
327.8 (3)	$(15/2^+)$	0.00102 (4)	0.001	493	510
347.799 (23)	$(5/2^+)$	0.0014 (4)	0.0014	250	250
359.628 (16)	$(7/2^+)$	$<$0.0006		$>$480	
365.814 (6)	$(7/2^+)$	0.0045 (5)	0.003	58	87
374.789 (10)	$(7/2^+)$	0.0027 (6)	0.0028	82	80
382.53 (5)	$(7/2^-,9/2,11/2^+)$	0.000057 (5)		3400	
425.891 (13)	$(9/2^+)$	0.00054 (4)	0.0004	166	220
427.93 (19)	$(5/2^+)$	0.00030 (4)	0.0003	300	290
436.772 (17)	$(7/2^-)$	0.00072 (5)		103	
465.437 (22)	$(5/2^-,7/2,9/2^+)$	0.000119 (15)		370	
478.65 (3)	$(7/2^+,9/2^+)$	0.000050 (6)		690	
513.401 (23)	$(5/2^+,7/2,9/2^+)$	0.000049 (3)		375	

TABLE II. (*Continued.*)

E_{level} (keV)	I^{π}	Feeding intensity (%) This work	Feeding intensity (%) From α spectra[a]	Hindrance factor This work	Hindrance factor From α spectra[a]
526.70 (4)	$(5/2^+,7/2^+)$	0.0008 (3)	0.0009	18	16
536.30 (11)	$(1/2^-)$	0.0000026 (11)		4600	
569.255 (18)	$(3/2,5/2^+)$	0.0000158 (24)		410	
585.09 (3)	$(5/2^+,7/2,9/2^+)$	0.0000083 (16)		580	
605.237 (23)	(5/2,7/2)	0.0000087 (13)		380	
620.79 (7)	$(5/2^+,7/2)$	0.0000073 (13)		340	
637.45 (4)	$(5/2^+,7/2,9/2^+)$	0.0000103 (15)		170	
656.92 (5)	$(5/2^+,7/2,9/2^+)$	0.0000061 (11)		200	
665.02 (10)	(1/2,3/2,5/2)	0.00000093 (23)		1100	
749.91 (8)	$(5/2^+,7/2,9/2^+)$	0.0000144 (21)		13.6	

[a]From Ref. [24].
[b]Includes contribution to the 0.0034-keV level.
[c]No clear evidence of γ-ray transition deexciting this level was found.
[d]Includes contribution to the 148.154-keV level.
[e]Includes contribution to the 164.530-keV level.
[f]Some intensity is missing: low energy transitions strongly internal-converted were not detected in γ spectrum.
[g]Includes contributions to the 235.347- and 241.557-keV levels.
[h]Includes contribution to the 288.472-keV level.

keV $(5/2^+)$. A Coriolis mixing calculation between this band and the $3/2^+[631]$ band, assuming $A=6.06$ keV obtained from the ground state band and using the first four levels (two for each band), gives a decoupling parameter $a=0.42$ for the $1/2^+[631]$ band and a Coriolis mixing matrix element $\langle 3/2[631]|\hat{j}_+|1/2[631]\rangle = 2.3$. This value disagrees with the 0.504 value of the Nilsson model theoretical calculation of Gustafsson *et al.* [55] for $\epsilon_2=0.2$ [56], or the -0.39 value of the calculation of Chasman *et al.* [51] for $\epsilon_2=0.19$ with a Woods-Saxon potential. The mixing strength is 2.9×10^{-2}. Incidentally the calculated energy of the $5/2^+$ level of the $1/2^+[631]$ band is 307.1 keV, which matches reasonably well with the experimental 317.176-keV $(5/2^+)$ level. Also, the decoupling parameter does not agree with the experimental values for the $1/2^+[631]$ band in the mass region $A>229$, which are negative, in the range -0.14 to -0.50, and with the theoretical value of -0.39 in the strong coupling limit [51]. This may be an indication of asymmetric effects (see Sec. IV B).

TABLE III. Summary of measured experimental reduced transition probabilities and calculated rotational model quadrupole moments and magnetic g factors.

E_γ (keV)	$K_f\ I_f$	δ	Experiment $B(M1)$ (μ_N^2)	Experiment $B(E2)$ ($e^2\,b^2$)	Rotational model Q_{20} (b)	Rotational model $\lvert g_K-g_R\rvert$
		From 42.434-keV level,[a] $7/2^+$, $T_{1/2}=0.172^{b}(6)$ ns				
42.434[c]	5/2 5/2	0.40[d,e] (10)	0.019[e] (6)	2.4[e] (13)	8.2[e] (22)	0.24[e] (4)
		From 97.137-keV level,[a] $9/2^+$ $T_{1/2}=0.147^{b}(12)$ ns				
25.311[f]	3/2 7/2	[0.0114][g]	0.0201 (24)	[0.0090[g] (11)]		
54.707[c]	5/2 7/2	0.46[d] (3)	0.0131 (20)	1.33 (25)	6.6 (6)	0.169 (13)
67.943[f]	3/2 5/2			0.049 (6)		
97.129[c]	5/2 5/2			0.52 (6)	7.2 (4)	
				Mean:	7.1 (3)	0.176 (21)

[a]Nilsson model: $5/2^+[633]$ band.
[b]From Ref. [41].
[c]Rotational model: intraband transition.
[d]From conversion electron measurements [22,24].
[e]Mixed with the 42.69-keV transition: unreliable value.
[f]Rotational model: interband transition.
[g]Calculated from Alaga's rule.

TABLE IV. Intraband transitions within the $5/2^+[633]$ band. Values in square brackets are calculated.

I_i	I_f	E_γ (keV)	$\lvert\delta\rvert$	$\left\lvert\frac{Q_{20}}{g_K-g_R}\right\rvert$ (b)
7/2	5/2	42.4344 (11)	0.40 (10)	34 (8)
9/2	7/2	54.7040 (11)	0.46 (3)	39 (3)
11/2	9/2	66.1135 (20)	0.56 (20)	49 (7)
13/2	11/2	78.10 (10)	[0.45 (3)]	
(15/2)	13/2	86.3[a] (2)	[0.43]	

[a]Multiply placed γ-ray transition.

4. Intraband and interband matrix elements and multiplet resolution between 5/2$^+$[633] and 3/2$^+$[631] bands

The close level spacing between the two bandheads raises the question of determining the correct intensities of the transitions between the lower states (Fig. 6).

The 42-keV multiplet was separated into the 42.43- and 42.69-keV γ's by spectroscopic methods, but the 29-keV line was not separated into 29.38- and 29.19-keV transitions and the 42.43, 29.19, and 71.82 keV are still doublets and should be resolved. No present state-of-the-art detector allows to separate these doublets. Helmer and Reich [2] assumed that intraband transitions were much more intense than interband transitions and were able to deduce the energy of the first excited level by carefully measuring γ-ray energy differences. We performed a calculation of intraband and interband transition intensities according to the strong coupling rotational model and verified to which extent their assumption was justified.

We define intrinsic matrix elements (m.e.) independent of spins [48] for $M1$ and $E2$ transitions. For intraband transitions these m.e. are $m(M1)=\mu_N(g_K-g_R)K$ and $m(E2)=eQ_{20}$. In first order approximation of unperturbed rotational bands, five intrinsic matrix elements should completely describe the transition probabilities: one quadrupole moment characterizing the whole deformation of the nucleus, two magnetic moments, one for each band, and two transitional electric quadrupole and magnetic dipole moments. From the decay of the 97.137-keV level we found 7.05 e b and $0.421\mu_N$ for the $5/2^+[633]$-band moments, and $1.22e$ b and $0.425\mu_N$ for the transitional moments, respectively. Assuming the same deformation for the $3/2^+[631]$ band as the g.s. band, and from the experimental intensity ratios of the $\Delta I=1$ and $\Delta I=2$ transitions issuing from the 125.425-keV level we calculated the intrinsic magnetic moment of the $3/2^+[631]$ band: $0.88\mu_N$. These values were used throughout in Table VI, combined with information derived from the experimental intensity ratios for two different transitions issued from the same level:

$$\frac{I_{\gamma1}}{I_{\gamma2}}=\frac{P_{\gamma1}(M1)+P_{\gamma1}(E2)}{P_{\gamma2}(M1)+P_{\gamma2}(E2)}=\frac{E_{\gamma1}^3}{E_{\gamma2}^3}\frac{B_1(M1)+0.697E_{\gamma1}^2B_1(E2)}{B_2(M1)+0.697E_{\gamma2}^2B_2(E2)}. \quad (2)$$

The calculated values for the low energy multiplets of Fig. 6 are reported in Table VII.

The assumption of Helmer and Reich [2] that the 29.19- and 71.81-keV γ rays should be mostly intraband transitions to the 3.4-eV level is not fully justified. The transition to the g.s. amounts to 25% for the former and to 40% for the latter. In our approach the α-particle feeding intensities to the level calculated from γ-ray imbalance at the levels agree reasonably well with the experimental α-particle measurements (Table II).

TABLE V. Intraband transitions within the $3/2^+[631]$ band. Values in square brackets are calculated.

I_i	I_f	E_γ (keV)	$\lvert\delta\rvert$	$\left\lvert\frac{Q_{20}}{g_K-g_R}\right\rvert$ (b)
(5/2)	(3/2)	29.1867 (11)	[0.152 (5)]	
(7/2)	(5/2)	42.6269 (11)	0.160 (6)	13.5 (5)
(9/2)	(7/2)	53.6104 (17)	0.132 (5)	11.6 (4)
(11/2)	(9/2)	70.282 (5)	0.157 (3)	12.97 (21)

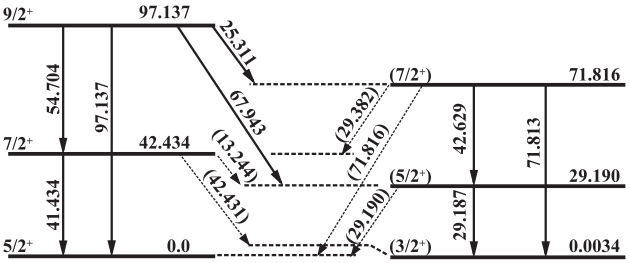

FIG. 6. The low energy multiplets.

5. Other bands

The negative parity bands $5/2^-$, starting at 146.35 keV, and $3/2^-$, starting at 164.53 keV, mainly decaying to the $3/2^+[631]$ band, were confirmed. They may be assigned to the $5/2^-[752]$ and $3/2^-[761]$ Nilsson configurations. The band parameters calculated from level energies are not significant: as shown by Kroger and Reich [17] these bands are strongly Coriolis mixed with the negative parity configurations arising from the $j_{15/2}$ shell (the $1/2^-[770]$ and $7/2^-[743]$ configurations).

The $1/2^+[631]$ band starting at 261.940 keV, proposed from (d,t) reaction studies [43,47], is confirmed. The identification of the $5/2^+$ member with the 317.176-keV level is proposed and agrees with the rotational formula; however, the α-particle decay hindrance factor does not agree very well.

The second $5/2^+$ band, starting at 320.54 keV, was interpreted as the β band, $5/2^+[633]\otimes 0^+$, in earlier studies [17], because of an enhanced α-particle decay hindrance factor. But the 0^+ excitation is considerably higher in energy in the

TABLE VI. Reduced transition probabilities and intrinsic matrix elements according to rotational model calculation. Experimental values are in bold type.

E_{level} (keV)	$I_i\ K_i\ I_f\ K_f$	E_γ (keV)	I_γ (%)	$B(E2)$ (e^2 b^2)	$\lvert m(E2)\rvert$[a] (e b)	$B(M1)$ (μ_N^2)	$\lvert m(M1)\rvert$[b] (μ_N)	$\lvert\delta\rvert$
0.0034	3/2 3/2 5/2 5/2	(0.0034)		0.063 (8)	[c]	0.043 (5)	[d]	0.0034 (18)
29.1904	5/2 3/2 3/2 3/2	**29.1867**	**7.8 (6)**	1.72 (16)	[e]	0.048 (5)	[f]	0.145 (10)
	5/2 5/2	29.190	2.5 (6)	0.064 (8)	[c]	0.0124 (15)	[d]	0.055 (5)
42.4341	7/2 5/2 5/2 5/2	**42.4344**	**72 (4)**	1.76 (18)	[e]	0.0090 (14)	[g]	**0.40 (10)**
	3/2 3/2	42.431	0.18 (5)	0.042 (5)	[c]			
	5/2 3/2	13.244	2.4 (7)	0.00175 (22)	[c]	0.023 (3)	[d]	0.0030 (3)
71.8158	7/2 3/2 3/2 3/2	**71.8133**	1.81 (14)	0.71 (7)	[e]			
	5/2 5/2	**71.8133**	1.16 (12)	0.026 (3)	[c]	0.00154 (19)	[d]	0.248 (22)
	5/2 3/2	**42.6296**	**13.2 (7)**	1.06 (11)	[e]	0.066 (8)	[f]	0.143 (12)
	7/2 5/2	29.382	0.80 (14)	0.045 (6)	[c]	0.0165 (20)	[d]	0.041 (4)
97.1371	9/2 5/2 5/2 5/2	**97.1376**	**20.3 (10)**	**0.52 (6)**	**7.2 (4)**			
	7/2 5/2	**54.7040**	**16.8 (8)**	**1.33 (25)**	**6.6 (6)**	**0.0131 (20)**	**0.42 (3)**	**0.46 (3)**
	5/2 3/2	**67.943**	**0.320 (23)**	**0.049 (6)**	**1.22 (8)**			
	7/2 3/2	**25.311**	**2.11 (12)**	0.00089 (11)	[c]	**0.0201 (24)**	**0.43 (3)**	0.0044 (4)
125.4252	9/2 3/2 5/2 3/2	**96.232**	**1.70 (9)**	1.06 (11)	[e]			
	7/2 3/2	**53.6104**	**3.47 (18)**	0.69 (7)	[e]	0.074 (9)	0.88 (5)	0.132 (10)
	7/2 3/2	**125.41**	**0.051 (10)**	0.0085 (19)	1.72 (23)			
	7/2 5/2	**83.000**	**0.197 (22)**	0.074 (17)	1.72[h] (23)	0.0009 (4)	0.25 (4)	0.64 (16)
	9/2 5/2	28.288	0.036 (9)	0.063 (14)	1.72[h] (23)	0.0056 (25)	0.23[i] (5)	0.079 (20)
163.2488	11/2 5/2 7/2 5/2	**120.8129**	**2.82 (15)**	0.84 (8)	[e]			
	9/2 5/2	**66.116**	**1.06 (6)**	1.5 (3)	8.1 (7)	0.015 (3)	0.41 (4)	0.56 (20)
	7/2 3/2	91.433	0.041 (7)	0.050 (6)	[c]			
	9/2 3/2	**37.823**	**0.25 (4)**	0.0048 (6)	[c]	0.0183 (22)	[d]	0.0162 (14)
195.702	11/2 3/2 7/2 3/2	**123.881**	**0.72 (5)**	1.26 (13)	[e]			
	9/2 3/2	**70.281**	**0.58 (4)**	0.48 (5)	[e]	0.058 (8)	0.75 (9)	0.170 (15)
	7/2 5/2	**153.13**	**0.037 (3)**	0.022 (3)	1.99 (15)			
	9/2 5/2	98.565	0.097 (16)	0.041 (5)	[c]	0.0039 (5)	[d]	0.267 (22)
	11/2 5/2	32.453	0.016 (3)	0.023 (3)	[c]	0.0193 (24)	[d]	0.029 (3)
241.557	11/2 5/2 9/2 5/2	**144.426**	**0.30 (3)**	1.07 (11)	[e]			
	11/2 5/2	**78.21**	**0.038 (7)**	0.89 (9)	[e]	0.011 (3)	0.33 (5)	0.60 (9)
	9/2 3/2	**116.3**	0.0089 (11)	0.047 (9)	[c]			
	11/2 3/2	45.855	0.0091 (16)	0.0088 (11)	[c]	0.0171 (21)	[d]	0.0275 (24)
272.5	13/2 3/2 9/2 3/2	**146.9**	**0.119 (10)**	1.38 (14]	[e]			
	11/2 3/2	**77.142**	**<0.43**	0.35 (4)	[e]	0.081 (10)	[f]	0.135 (11)
327.8	15/2 5/2 11/2 5/2	164.5	0.261 (5)	1.22 (13)	[e]			
	13/2 5/2	**86.3**	0.038 (3)	0.70 (7)	[e]	0.0171 (20)	[g]	0.45 (4)
	11/2 3/2	132.1	0.0035 (7)	0.049 (6)	[c]			

[a]For intraband transitions identical to eQ_{20}.
[b]For intraband transitions identical to $K(g_K-g_R)\mu_N$.
[c]Assumed reference: interband intrinsic $\lvert m(E2)\rvert=1.22\pm0.08$ e b, from the 67.943-keV transition.
[d]Assumed reference: interband intrinsic $\lvert m(M1)\rvert=(0.42\pm0.03)\mu_N$, from the 54.704-keV transition.
[e]Assumed reference: same intraband $\lvert m(E2)\rvert=7.1\pm0.3$ e b, for the two bands; mean from the 97.137- and 54.704-keV transitions.
[f]Assumed reference: intraband $3/2^+[631]$ $\lvert m(M1)\rvert=(0.88\pm0.05)\mu_N$, from the 53.610-keV transition.
[g]Assumed reference: intraband $5/2^+[633]$ $\lvert m(M1)\rvert=(0.42\pm0.03)\mu_N$, from the 54.704-keV transition.
[h]From the 125.41-keV transition, from the same level.
[i]From the 83.0-keV transition, from the same level.

even-even neighboring nuclei (831.823 keV in ^{228}Th and 643.9 keV in ^{230}Th). The configuration $5/2^+[622]$ is not too far away and could mix into the $5/2^+$ band.

A $1/2^-$ band, starting at 536.30 keV, was proposed by (d,t) reaction measurements and identified as the $1/2^-[501]$ configuration [47]. In the odd deformed nuclei with mass $A>229$, this configuration was observed with a decoupling factor ≈0.8. With an inertia parameter $A\approx6$ keV and such a decoupling factor, the levels at 569.25 and 605.24 keV could be the $3/2^-$ and $5/2^-$ members.

TABLE VII. Analysis of the low energy multiplets.

Experiment			Deconvolution			Transition
E_γ (keV)	I_γ	δ	E_γ (keV)	I_γ	δ	$E_i - E_f$ (keV)
29.1867 (11)	11.3 (10)	[a]	29.1867	7.8	0.145	29.190–0.0034
			(29.190)	2.7	0.055	29.190–0
			(29.382)	0.80	0.041	71.816–43.43
42.4344 (11)	72.0 (36)	0.40[b] (10)	43.434	72.0	0.43	42.434–0
			(42.431)	0.18	[c]	42.434–0.0034
42.6296 (21)	13.2 (7]		42.6296	13.2	0.143	71.816–29.190
71.8133 (16)	2.97 (15)	[a]	71.833	1.81	[c]	71.816–0.0034
			(71.816)	1.16	0.248	71.816–0

[a]Unknown or not measured.
[b]Total 42.434+42.630.
[c]$E2$ multipolarity.

The band proposed from earlier studies on α-particle decay [42] at 21, 75, and 140 keV and assigned as the $7/2^-[743]$ configuration is uncertain. Some weak transitions might well be assigned to this band, but all of them appear to be hidden into multiplets so that no clear assignment could be given. Moreover, this band should be strongly mixed by Coriolis interaction with the other configurations issuing from the $j_{15/2}$ shell (see the beginning of this section), and the inertia parameter could not be equal to that of the g.s. band, as implied by the present assignment. These facts cast serious doubt on the reality of the band, and on the identification of the α-particle groups as ^{233}U emissions.

B. Reflection-asymmetric models

Several experimental features suggest that the ^{229}Th nucleus should be octupole deformed, either statically or dynamically.

(1) The $K=0^-$ octupole band is rather low in energy in the neighboring even-even nuclei ^{228}Th and ^{230}Th: the 1^- band head is at 328.0 keV in the former and at 508.2 keV in the latter, much lower than the first quadrupole deformed state 0^+ at 831.8 and 643.9 keV, respectively. The calculated energy of octupole deformation, defined formally as the energy of the virtual 0^- state

$$E(0^-) = E(1^-) - \frac{\hbar^2}{I}, \tag{3}$$

and weighted between the neighboring nuclei, is $\sim$392 keV.

(2) The negative parity bands preferentially deexcite towards the $3/2^+$ band starting at 3.4 eV; these bands, known to be strongly Coriolis mixed [17], should contain a significant contribution of the $3/2^-$ band starting at 164.53 keV, which could be the octupole deformed doublet of the $3/2^+$ band.

(3) The positive value of the decoupling parameter of the $1/2^+$ band (Sec. IV A 3) disagrees with the negative trend of the same band in heavier well-deformed nuclei, but agrees with the values in lighter nuclei (e.g., in ^{225}Ra: $a=1.3$ [30]).

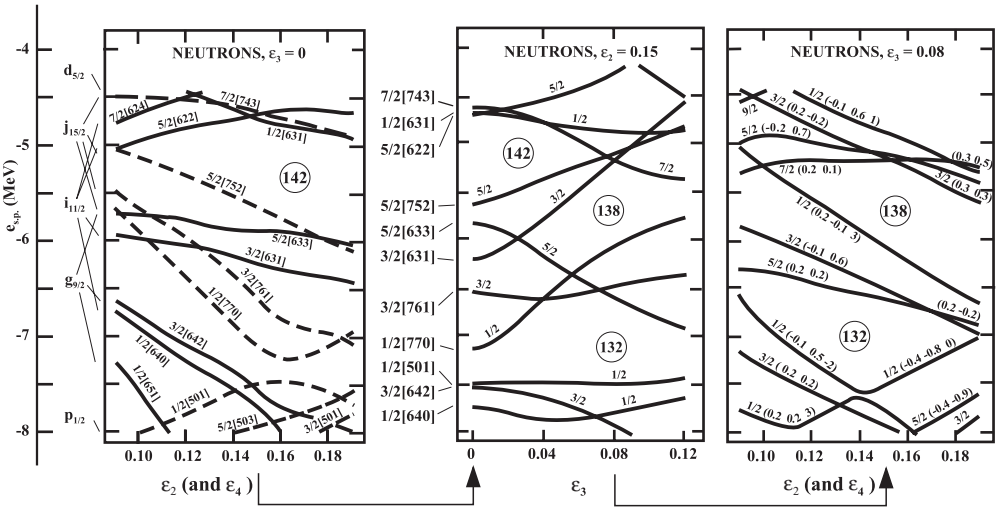

FIG. 7. Single particle energies of neutron orbitals in axially symmetric, but reflection-asymmetric folded Yukawa potential, against the quadrupole deformation ϵ_2 and octupole deformation ϵ_3. For labeling of orbitals see text. Good parity orbitals are drawn as broken lines for negative parity and as full lines for positive parity, respectively. The arrows show the connections between the sections.

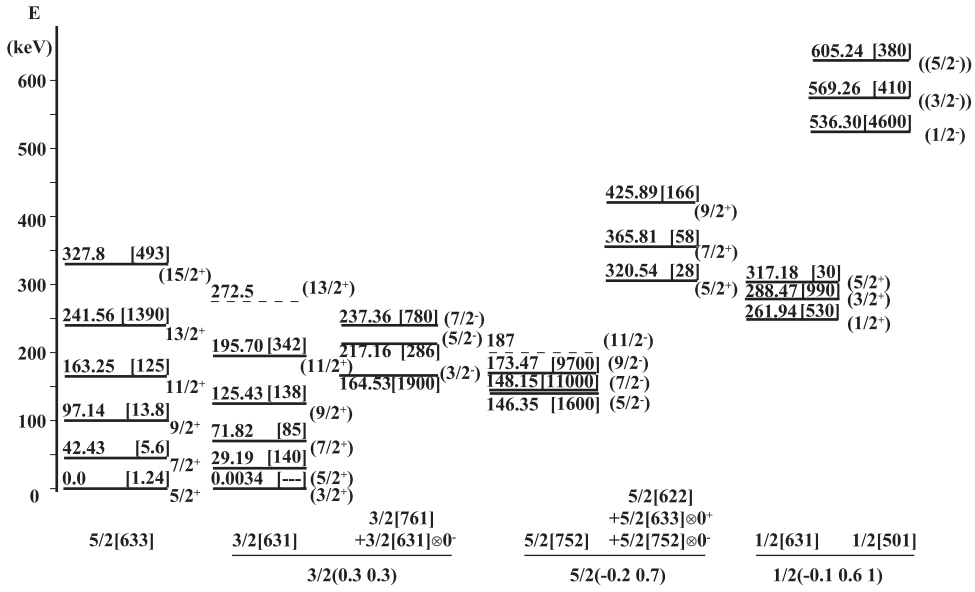

FIG. 8. Structure of bands assembled in parity doublets according to the configuration scheme of Fig. 7. Hindrance factors are given in square brackets at the levels. Nilsson asymptotic assignments are also given.

(4) The Nilsson model could account for the g.s. assignment of the $5/2^+[633]$ configuration, at $\epsilon_2 \approx 0.2$ [51], and the $3/2^+[631]$, $1/2^-[501]$, $5/2^-[752]$, and $3/2^-[761]$ configurations are also very close in energy, but the virtual crossing of the $3/2^+[631]$ and $5/2^+[633]$ configurations is difficult to obtain without an octupole deformation.

Early calculations in the framework of an octupole deformed core strongly coupled to single particle states have achieved a better agreement with a low ($\epsilon_3 \sim 0.04$) octupole deformation: Leander and Chen [8] with a Woods-Saxon potential and Ragnarsson [14] with a Nilsson potential, respectively.

We performed a calculation in the framework of a static octupole deformation between collective octupole modes and single quasiparticle degrees of freedom. The nuclear potential is an axially symmetric, but reflection-asymmetric folded Yukawa potential with quadrupole and octupole deformations. In Fig. 7 the level diagram for single neutron orbitals is plotted against quadrupole and octupole deformations: in the left-hand section versus ϵ_2, for $\epsilon_3 = 0$; in the center versus ϵ_3, for $\epsilon_2 = 0.15$; and in the right-hand section versus ϵ_2, for $\epsilon_3 = 0.08$. The orbitals are labeled, respectively, for $\epsilon_3 = 0$, by Nilsson asymptotic configurations, with indication of the spherical shell of origin, for $\epsilon_3 \neq 0$, by $\langle \hat{j}_z \rangle$, the good quantum number of the projection of the intrinsic angular momentum, and, on the right hand section, in parentheses, by the single particle matrix elements $\langle \hat{s}_z \rangle, \langle \hat{\pi} \rangle$, of the intrinsic spin and parity. For $K = 1/2$ bands, by the additional matrix element $\langle \hat{\pi} \chi_{1/2} | -\hat{j}_+ | \hat{R} \chi_{1/2} \rangle$ is also given, where $\hat{R}$ is the rotation operator by 180° around the symmetry axis, corresponding to the decoupling parameter of reflection-symmetric models times total parity. Neutron numbers are given in circles at gaps.

The main characteristic features of the model are the following predictions.

(1) Enhanced $E1$ transitions take place between parity doublet levels.

(2) The energy difference between doublet levels is

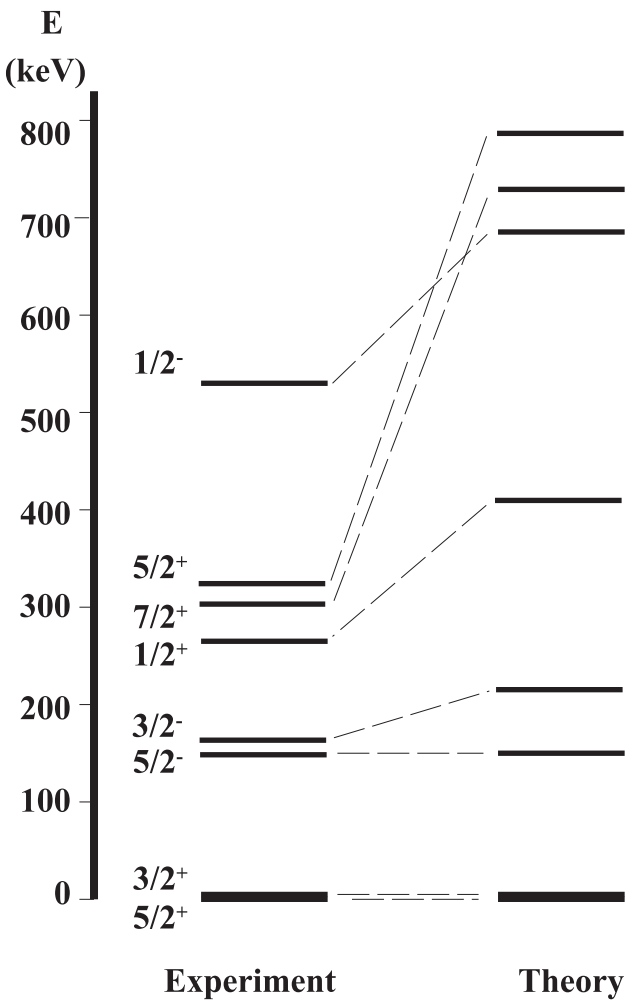

FIG. 9. Comparison of experimental and theoretical schemes of bandheads. Parameters are $\epsilon_2 \sim 0.15$ and $\epsilon_3 \sim 0.03$ as in Fig. 7.

$$E_{I_-} - E_{I_+} = \langle \hat{\pi} \rangle E_{0^-}, \quad (4)$$

for degenerate opposite-parity single-particle configurations.

(3) For $K=1/2$ bands the extended decoupling factor $\langle \hat{\pi}\chi_{1/2}|-\hat{j}_+|\hat{R}\chi_{1/2}\rangle$ should be equal for parity doublet bands.

From Fig. 7, we can see that 3/2, 5/2, and 7/2 configurations cross at $\epsilon_2 \sim 0.15$ and $\epsilon_3 \sim 0.03$–0.08. There is a minimum for the Fermi level, following the $N=139$ neutron orbital, for $\epsilon_2 \sim 0.15$ and $\epsilon_3 \sim 0.03$, where the 5/2 and 3/2 orbitals cross. The orbital scheme is quite independent of the potential and follows the same trends for folded Yukawa (this work), Nilsson [14], and Woods-Saxon potentials [8].

The g.s. band could be assigned to the 5/2(0.2 0.2) configuration, which goes up rapidly when ϵ_3 decreases, but does not seem to have an experimental parity partner, and could be almost pure $5/2^+[633]$ configuration. This would imply that there is a coexistence of octupole-deformed and normal Nilsson-deformed bands and has already been proposed for a remarkably similar level structure in ^{227}Ra [58]. Leander and Chen [8], quoting a paper of Bemis *et al.* [50], who performed Coulomb excitation measurements, assigned the parity partner to a band starting at 512 keV. No evidence of these levels was found in this work. Conversely, two levels at 235.35 (probable $5/2^-$) and 287.87 keV ($7/2^-$) might be the members of this band. But these levels do not show a preferred decay to the levels of the g.s. band, so this identification is very doubtful. The spectroscopic quadrupole moment and magnetic dipole moment calculated in the framework of the asymmetric model, $Q=2.88$ b and $\mu=0.63\mu_N$ [8], are not in much better agreement with the experimental values than that deduced from the strong coupling symmetric model, and do not change significantly.

The $3/2^+$ band starting at 3.4 eV and the $3/2^-$ band starting at 164.53 keV are connected by strong $E1$ transitions. It was already proposed [17] that the latter could contain a significant component of the octupole vibration: $3/2^+[631] \otimes 0^-$. In our interpretation they would belong to the 3/2(0.3 0.3) parity doublet.

The parity partner of the $5/2^-$ band starting at 146.35 keV could be the $5/2^+$ band starting at 320.54 keV. A second 5/2(−0.2 0.7) orbital lies in this region. The positive parity band decays to the parity partner with transitions of significant intensity. In a dynamical approach it could contain a contribution from the coupling $5/2^-[752]\otimes 0^-$, of the Nilsson deformed orbital with the octupole vibration.

The configuration 7/2(0.2 0.1) band is also expected at low excitation energy. The existence of a low energy $7/2^-$ band proposed in some α-particle studies is thus supported by the model, but at greater ϵ_3 and lower ϵ_2 deformations, and its existence is not clearly established in this work. It should also be noted that the g.s. of ^{225}Rn, an isotone of ^{229}Th, has been measured to be $7/2^-$ [59], as expected for an $N=139$ nucleus with somewhat smaller ϵ_2 and higher ϵ_3. Another level at 302.98 keV, assigned as $7/2^+$ in this work from decay properties, may be the parity doublet bandhead.

The $1/2^+$ band, starting at 261.94 keV, and the $1/2^-$ band, starting at 536.30 keV, might be assigned to the 1/2(−0.1 0.61) configuration. The experimental decoupling parameter of the positive parity band agrees in sign with the calculated one.

TABLE VIII. Comparison of calculated and experimental $\langle \hat{\pi} \rangle$.

I^π (Band head)	$E_{\rm exp}$ (keV)	$\langle \hat{\pi} \rangle_{\rm exp}$	$\langle \hat{\pi} \rangle_{\rm th}$ a	b	c
$5/2^+$	0.0	0.60	−0.1	0.2	0.71
$3/2^+$	0.0034	0.42	0.2	0.3	0.74
$5/2^-$	146.35	−0.44	0.6	0.7	−0.26
$1/2^+$	261.94	0.70	0.7	0.6	0.90

[a] $\beta_2=0.18$ ($\epsilon_2 \sim 0.17$), $\beta_3=0.10$ ($\epsilon_3 \sim 0.075$) [8].
[b] $\epsilon_2=0.16, \epsilon_3=0.08$ present work.
[c] $\epsilon_2=0.18, \epsilon_3=0.04$ [14].

The evolution of the different configurations for the isotonic nuclei with $N=139$ is poorly known. Except for ^{227}Ra the experimental data are very scanty. However, the structure of ^{227}Ra has been studied using (n,γ), (d,p), (d,t) reactions and β decay [57]. There are great similarities with ^{229}Th, with $3/2^+$ as g.s. and $5/2^+$ as excited state at 1.735 keV, and $3/2^\pm$ and $1/2^\pm$ low lying parity doublet bands [58].

The bands are assembled in parity doublets in Fig. 8 according to the theoretical allowed configurations of Fig. 7.

With the calculation of Fig. 7 for a parameter set $\epsilon_2 \sim 0.15$ and $\epsilon_3 \sim 0.03$, with quasiparticle energies, Fermi level at the $N=139$ orbital, and pairing gap $\Delta = Z/A$, the theoretical scheme of bandheads is compared to the experimental one in Fig. 9.

The agreement is rather good for the four first bands. For the $1/2^\pm$ bands the increase of the octupole deformation, ϵ_3, brings the configurations to lower excitation energies and exchanges parities, in much better agreement with experiment (Fig. 7). Also the 7/2 orbital is lowered at higher ϵ_3 and the lowest member acquires positive parity.

In Table VIII we have compared the values of the intrinsic parity $\langle \hat{\pi} \rangle$ [Eq. (4)] deduced from the experimental energy differences for the bandheads and calculated by different authors. The agreement is better for the calculation by Ragnarsson [14] with $\epsilon_2=0.18$ and $\epsilon_3=0.004$.

Finally, it should be noted that present experimental data do not permit to clearly discriminate between symmetric and asymmetric models. However, the asymmetry is low and might affect only moderately the parameters. Conversely, there are clear indications that shape coexistence should play a leading role, not only between symmetric and asymmetric configurations, but also between different deformations. The deformations parameters should be optimized for every level. Configuration mixing calculations should give the best results.

V. CONCLUSIONS

Using continuously purified sources ~70 new γ transitions out of a total of ~220 are observed in ^{229}Th following the α decay of ^{233}U.

Accurate measurements of γ-ray spectra combined with theoretical estimations from a crude rotational scheme have

allowed a good agreement of α-particle feeding intensities to the levels from γ imbalances with measured experimental values.

Theoretical calculations in the framework of the rotational strong coupling symmetric model are in reasonable agreement with observed magnetic moments and gyromagnetic ratios. Nevertheless, a better agreement can be achieved if a small asymmetric deformation is introduced. Parity doublet bands can be assigned and signatures of asymmetric effects identified. Coexistence of reflection symmetric and asymmetric bands is present: the g.s. band is almost purely symmetric and the associated parity doublet is not clearly observed.

Because of the lack of interpretation of so many of the levels the study of ^{229}Th is still a formidable challenge. Careful observation of the internal conversion electron spectrum of ^{229}Th would be of great value. Coulomb excitation and inelastic scattering of ^{229}Th should help to identify more states associated with the $5/2^+$ ^{229}Th ground state.

However, the greater challenge is to theorists. In a transition nucleus, such as ^{229}Th, different rotational bands will have different parameters corresponding to different nuclear shapes. The variation between bands will probably be greater than the reflection symmetric and reflection asymmetric we have already identified in ^{229}Th. Up to the present time all we can do is use different parameters for the nucleus as a whole. A first step would be the complete evaluation of a three-dimensional model of ϵ_2, ϵ_3 versus energy. Ultimately we would have to hope that a much more profound nuclear model would take the different bands into account from first principles, without so many adjustable parameters. However, this kind of a nuclear model is nowhere on the horizon at present.

ACKNOWLEDGMENTS

It is a pleasure to thank Philippe Abela for technical assistance. One of us (R.K.S.) also thanks the state of Florida for support.

[1] C.W. Reich and R.G. Helmer, Phys. Rev. Lett. **64**, 271 (1990).
[2] R.G. Helmer and C.W. Reich, Phys. Rev. C **49**, 1845 (1994).
[3] P. Kálmán and T. Keszthelyi, Phys. Rev. C **49**, 324 (1992).
[4] S.B. Utter, P. Beiersdorfer, A. Barnes, R.W. Lougheed, J.R. Crespo López-Urrutia, J.A. Becker, and M.S. Weiss, Phys. Rev. Lett. **82**, 505 (1999).
[5] E.V. Tkalya, A.N. Zherikhin, and V.I. Zhudov, Phys. Rev. C **61**, 064308 (2000).
[6] G.A. Leander, R.K. Sheline, P. Möller, P. Olanders, and I. Ragnarsson, Nucl. Phys. **A388**, 452 (1982).
[7] G.A. Leander and R.K. Sheline, Nucl. Phys. **A413**, 375 (1984).
[8] G.A. Leander and Y.S. Chen, Phys. Rev. C **37**, 2744 (1988).
[9] R.K. Sheline, A.K. Jain, K. Jain, and I. Ragnarsson, Phys. Lett. B **219**, 47 (1989).
[10] R. Piepenbring, Z. Phys. A **323**, 341 (1986).
[11] P.A. Butler and W. Nazarewicz, Nucl. Phys. **A535**, 249 (1991).
[12] V.Y. Denisov and A.Y. Dzyublik, Nucl. Phys. **A589**, 17 (1995).
[13] R.R. Chasman, Phys. Lett. **96B**, 7 (1980).
[14] I. Ragnarsson, Phys. Lett. **130B**, 352 (1983).
[15] R. Piepenbring, J. Phys. (Paris), Lett. **45**, L1023 (1984).
[16] R.R. Chasman, Phys. Lett. B **175**, 254 (1986).
[17] L.A. Kroger and C.W. Reich, Nucl. Phys. **A259**, 29 (1976).
[18] M.J. Canty, R.D. Connor, D.A. Dohan, and B. Pople, J. Phys. G **3**, 421 (1977).
[19] I. Ahmad, Nucl. Instrum. Methods Phys. Res. A **223**, 319 (1984).
[20] K.M. Glover, Int. J. Appl. Radiat. Isot. **35**, 239 (1984).
[21] A. Lorenz, IAEA Report No. 261, 1986 (unpublished).
[22] E.F. Tretyakov, M.P. Anikina, L.L. Goldin, G.I. Novikova, and N.I. Pirogova, Zh. Éksp. Teor. Fiz. **37**, 917 (1959) [Sov. Phys. JETP **10**, 656 (1960)].
[23] R.S. Hager and E.C. Seltzer, At. Data Nucl. Data Tables **A6**, 1 (1969).
[24] Y.A. Akovali, Nucl. Data Sheets **59**, 263 (1990).
[25] A. Koua-Aka, G. Ardisson, V. Barci, O. El Samad, D. Trubert, I. Ahmad, Nucl. Instrum. Methods Phys. Res. A **369**, 477 (1996).
[26] G. Ardisson, A.A. Koua, V. Barci, C. Marsol, and G. Barci-Funel, Radiochim. Acta **78**, 15 (1997).
[27] P. Dali-Tepko, V. Barci, P. Abela, and G. Ardisson, J. Radioanal. Nucl. Chem. **250**, 69 (2001).
[28] C. Kouassi, C. Ardisson-Marsol, and G. Ardisson, J. Phys. G **16**, 1881 (1990).
[29] J. Gasparro, G. Barci-Funel, and G. Ardisson, Radiochim. Acta **83**, 1 (1998).
[30] J. Gasparro, G. Ardisson, V. Barci, and R.K. Sheline, Phys. Rev. C **62**, 064305 (2000).
[31] G. Ardisson, J. Gasparro, V. Barci, and R.K. Sheline, Phys. Rev. C **62**, 064306 (2000).
[32] J. Gasparro, G. Ardisson, V. Barci, and J. C. Abbé, in *Fifth Workshop on Nuclear Physics*, *WONP 99* (La Habana, Cuba, 1999).
[33] G. Ardisson, V. Barci, and O. El-Samad, Phys. Rev. C **57**, 612 (1998).
[34] R. B. Firestone, V. S. Shirley, C. M. Baglin, S. Y. F. Chu, and J. Zipkin, *Table of Isotopes*, 8th ed. (Wiley, New York, 1996).
[35] R. Gunnink and J. B. Niday, Lawrence Livermore National Laboratory Report UCRL-51061 (unpublished).
[36] J. K. Tuli, Brookhaven National Laboratory Report BNL-NCS-51655-01/02-Rev, http://www.nndc.bnl.gov/nndc/ensdfpgm/
[37] M.A. Preston, Phys. Rev. **71**, 865 (1947).
[38] C.W. Reich, R.G. Helmer, J.D. Baker, and R.J. Gehrke, Int. J. Appl. Radiat. Isot. **35**, 185 (1984).
[39] R.G. Helmer, C.W. Reich, M.A. Lee, and I. Ahmad, Int. J. Appl. Radiat. Isot. **37**, 139 (1986).
[40] G. Audi and A.W. Wapstra, Nucl. Phys. **A595**, 409 (1995).
[41] H. Ton, S. Roodbergen, J. Brasz, and J. Blok, Nucl. Phys. **A155**, 245 (1970).
[42] S.A. Baranov, M.K. Gadzhiev, V.M. Kulakov, and V.M. Shatinskii, Yad. Fiz. **5**, 518 (1967); Sov. J. Nucl. Phys. **5**, 365 (1967).

[43] D.G. Burke, P.E. Garrett, T. Qu, and R.A. Naumann, Phys. Rev. C **42**, R499 (1990).
[44] K. Chayawattanangkur, G. Herrmann, and N. Trautmann, J. Inorg. Nucl. Chem. **35**, 3061 (1973).
[45] I. Ahmad, J.E. Gindler, A.M. Friedman, R.R. Chasman, and T. Ishii, Nucl. Phys. **A472**, 285 (1987).
[46] Y.A. Akovali, Nucl. Data Sheets **58**, 555 (1989); **61**, 187(E) (1990).
[47] J. R. Erskine (private communication).
[48] A. Bohr and B. Mottelson, *Nuclear Structure* (Benjamin, New York, 1975), Vol. 2.
[49] S. Gerstenkorn, P. Luc, J. Verges, D.W. Engelkemeier, J.E. Gindler, and F.S. Tomkins, J. Phys. (Paris) **35**, 483 (1974).
[50] C.E. Bemis, Jr., F.K. McGowan, J.L.C. Ford, Jr., W.T. Milner, R.L. Robinson, P.H. Stelson, G.A. Leander, and C.W. Reich, Phys. Scr. **38**, 657 (1988).
[51] R.R. Chasman, I.A. Ahmad, A.M. Friedman, and J.R. Erskine, Rev. Mod. Phys. **49**, 833 (1977).
[52] A. Artna-Cohen, Nucl. Data Sheets **80**, 723 (1997).
[53] Y.A. Akovali, Nucl. Data Sheets **69**, 155 (1993).
[54] S.G. Malmskog and M. Höjeberg, Ark. Fys. **35**, 197 (1967).
[55] C. Gustafsson, I.-L. Lamm, B. Nilsson, and S.G. Nilsson, Ark. Fys. **36**, 613 (1967).
[56] M.E. Bunker and C.W. Reich, Rev. Mod. Phys. **43**, 349 (1971).
[57] R.K. Sheline, Int. J. Mod. Phys. E **2**, 657 (1993).
[58] R. Neugart, E. Arnold, W. Borchers, G. Ulm, and K. Wendt, in *Proceedings of the 5th International Conference on Nuclei Far from Stability, Rosseau Lake, Canada, 1987*, edited by I. S. Tower (American Institute of Physics, New York, 1988), p. 126.
[59] T. von Egidy *et al.*, Nucl. Phys. **A365**, 26 (1981).